NASA TECHNICAL NOTE

NASA TN D-4695

C.1

NASA TN D-4695

DILUTION-JET MIXING STUDY FOR GAS-TURBINE COMBUSTORS

by Carl T. Norgren and Francis M. Humenik

Lewis Research Center
Cleveland, Ohio

NATIONAL AERONAUTICS AND SPACE ADMINISTRATION • WASHINGTON, D. C. • AUGUST 1968

DILUTION-JET MIXING STUDY FOR GAS-TURBINE COMBUSTORS

By Carl T. Norgren and Francis M. Humenik

Lewis Research Center
Cleveland, Ohio

NATIONAL AERONAUTICS AND SPACE ADMINISTRATION

For sale by the Clearinghouse for Federal Scientific and Technical Information
Springfield, Virginia 22151 – CFSTI price $3.00

ABSTRACT

An experimental mixing study was undertaken to evaluate various dilution-jet entries. Thirteen geometries including four geometric variations on rectangular diluent jets with flush openings, attached scoops immersed in the diluent air stream, attached chutes immersed in the hot air stream, and a single geometry incorporating flush circular holes were investigated. Diluent and hot streams with a velocity ratio from 0.55 to 2.20 (diluent stream Mach range 0.082 to 0.232) were introduced into the rectangular configuration exhausting directly to the atmosphere. The mixed-stream exhaust temperature was in the order of 750° to 975° R (417 to 542 K). Test conditions were representative to scaled-engine operation by geometric, velocity, and Reynolds number similarity.

STAR Category 01

DILUTION-JET MIXING STUDY FOR GAS-TURBINE COMBUSTORS

by Carl T. Norgren and Francis M. Humenik

Lewis Research Center

SUMMARY

An experimental mixing study was undertaken to evaluate various dilution-jet entry schemes to achieve acceptable outlet-temperature profiles for short-length combustors. Diluent and hot streams with a velocity ratio from 0.55 to 2.20 (diluent-stream Mach range, 0.082 to 0.232) were introduced into a rectangular configuration exhausting directly to the atmosphere. The mixed-stream exhaust temperature was in the order of 750° to 975° R (417 to 542 K). Test conditions were representative to scaled-engine operation by geometric, velocity, and Reynolds number similarity. Outlet-temperature profiles were obtained for rectangular-slot configurations with (1) flush openings, (2) attached scoops immersed in the diluent-air stream, and (3) attached chutes immersed in the hot-air stream. The geometry of the rectangular slots was further varied in four patterns. A single geometry incorporating flush circular holes was also included for a total of 13 different geometries, all of which had nominally equal total open hole area. The four basic pattern variations used with rectangular slots consisted of two different slot spacings (One spacing was equivalent to the turbine blade height, and the other spacing to one-half the turbine blade height.) with the row of slots in the upper plate either in line or staggered with respect to the lower plate to allow reinforcement or interleaving of the jets. Marked differences in both the degree of mixing and the apparent nature of the mixing process were encountered.

INTRODUCTION

The combustor exit-temperature profile is one of the most important factors in the development of advanced turbojet engines. An experimental study to evaluate various dilution-jet entry schemes to achieve desired outlet-temperature profiles for short-length combustors is reported herein. The desired temperature profile is determined from stress and structural considerations in the first-stage turbine stator and rotor. The degree to which the desired profile can be obtained in the actual combustor determines the life of the turbine at the design operating condition. As turbine blades are designed to operate at higher metal temperatures, the problem becomes increasingly critical. At very high design metal temperatures a poor combustor profile will produce accelerated deterioration.

High combustor-exit temperature is even more critical as applied to high bypass ratio engines because high temperature is coupled with high internal gas pressure. To reduce structural loading, it is desirable to reduce the physical dimensions of the combustor. The combustor diameter is usually controlled by compressor or turbine considerations; however, combustor length is a design variable. At high pressures theoretical combustion volumes are small (ref. 1) so that combustor length is governed primarily by dilution-jet mixing.

It is generally accepted that the quality of the outlet-temperature profile is dependent on the number of dilution jets and on the effectiveness of penetration (ref. 2). Aerodynamic mixing studies have provided a basis for predicting the performance of single-entry port systems, however, very little information is available on the effect of multiple and opposed jet penetration. Addititional information on this aspect of dilution-air handling is required in order to reduce the tedious trial and error tailoring of the dilution jets which is currently required to match combustor outlet-temperature profiles to turbine inlet requirements (ref. 3).

In this experimental program a simple rectangular mixing section was designed to simulate a segment of the diluent zone of an annular combustor. The mixing section was directly exhausted to the atmosphere, and operating conditions were simulated by maintaining Reynolds number and velocity similar to that which could be attained in an actual engine. Outlet-temperature profiles were obtained for a series of diluent-mixing plates incorporating rectangular-slot configurations with (1) flush openings, (2) attached scoops immersed in the diluent-air stream, and (3) attached chutes immersed in the hot-air stream. The geometry of the rectangular slots was varied in four patterns. The four basic pattern variations consisted of two different slot spacings (One spacing was equivalent to the turbine blade height, and the other spacing to one-half the turbine blade height.) with the row of slots in the upper plate either in line or staggered with respect to the lower plate to allow reinforcement or interleaving of the jets. A single geometry incorporating flush circular holes was also included for a total of 13 different geometries, all of which had nominally equal total open hole area. The individual hole characteristics were selected on the basis of existing hole discharge data and jet-penetration studies (refs. 1 and 4 to 8). Exit-temperature and total-pressure profile data were obtained for a parametric set of test conditions based on variations in proportioning the mass flow to the hot- and diluent-gas streams, in total mass flow to the mixing section, and in the temperature of the hot-gas stream.

DESIGN CONSIDERATIONS

Basic Test Selection

A simple rectangular mixing section (fig. 1) was designed to simulate the diluent-air

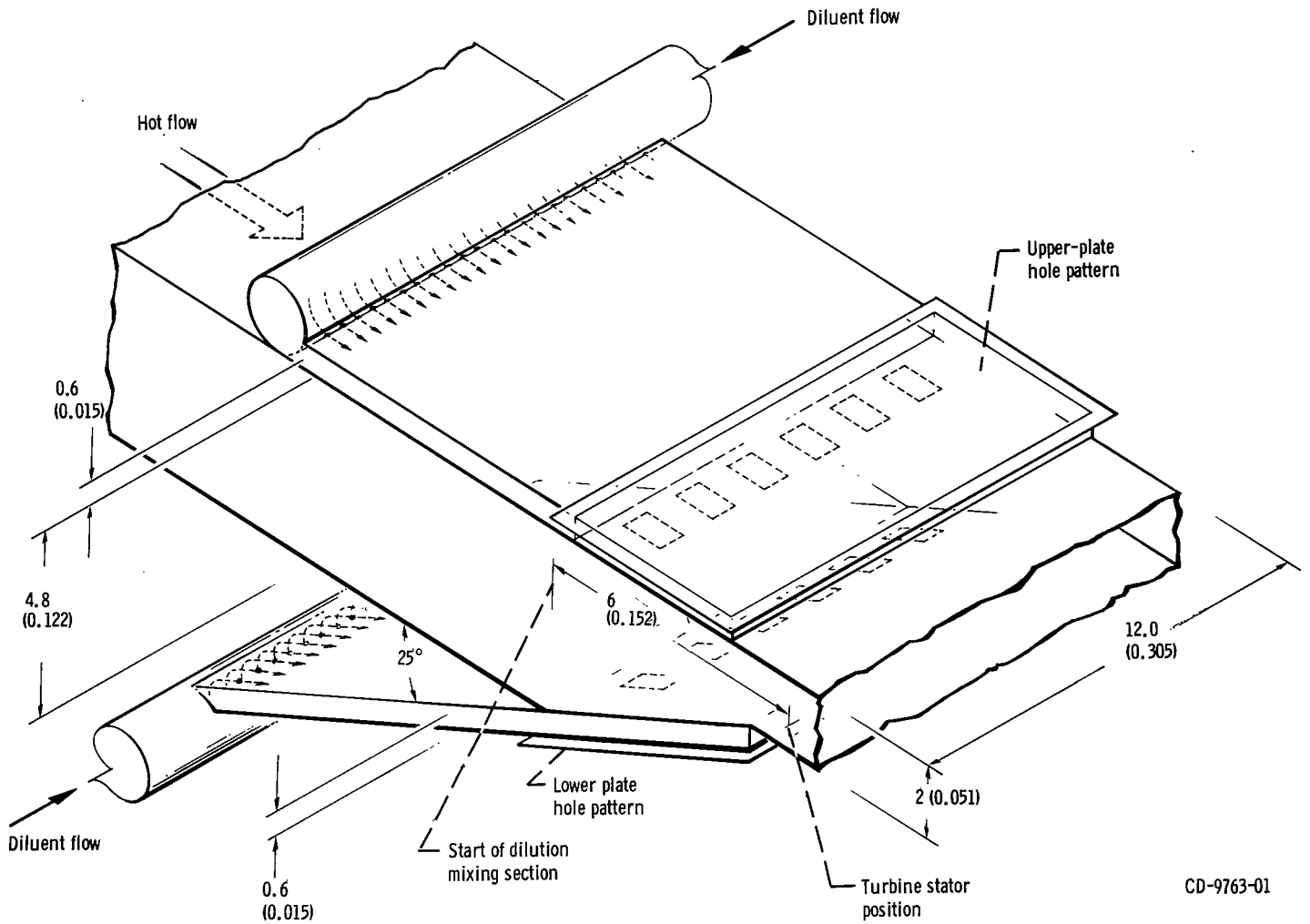

Figure 1. - Rectangular mixing section. (Linear dimensions are in inches (m).)

mixing zone of a segment of an annular turbojet combustor. The dimensions of the rectangular mixing section were taken to be similar to that of a short combustor suitable for a high-pressure-ratio engine. The rectangular shape was chosen because fabrication is simplified compared with that required to produce a sector of an annulus. The hot-combustion-gas stream is simulated by a hot-air stream in the center passage of the mixing section. The diluent-air streams were separately controlled and air was distributed equally between the upper and lower passages which correspond to the outer and inner walls of annular configuration.

The mixing process and, hence, the outlet-temperature profile depends on the penetration of the dilution jets and the subsequent turbulent mixing. It is shown in reference 1 that single-hole penetration data from several sources, in which the jet is injected normal to the stream, can be correlated in the form

$$\frac{Y}{d_j} = k_1 \left(\frac{\rho_{dil}}{\rho_h}\right)^{a_1} \left(\frac{U_j}{U_h}\right)^{b_1} \left(\frac{x}{d_j}\right)^{c_1} \tag{1}$$

(All symbols are defined in the appendix.) The geometry is defined in sketch (a). For a

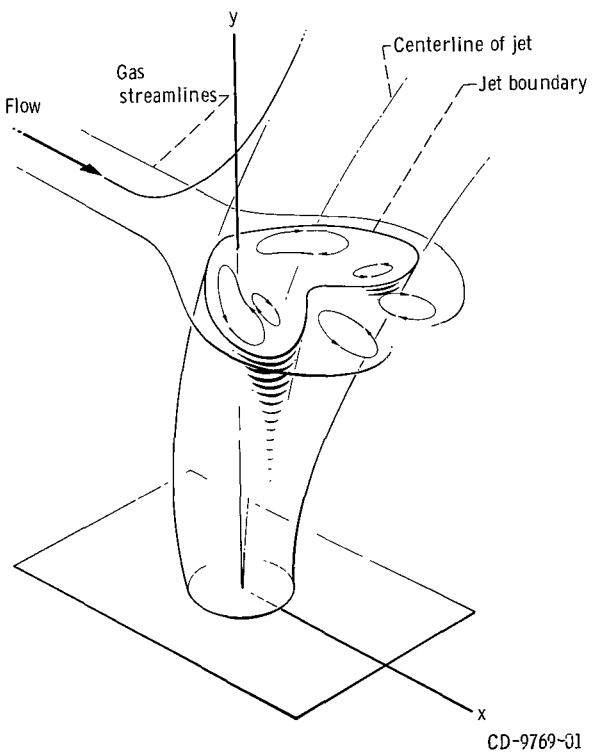

(a)

fixed geometry, sufficiently large diluent-stream Reynolds numbers, and low Mach numbers, this equation can be written

$$\frac{Y}{d_j} = k_2\left(\frac{\rho_{dil}}{\rho_h}\right)^{a_2}\left(\frac{U_{dil}}{U_h}\right)^{b_2}\left(\frac{x}{d_j}\right)^{c_2} \tag{2}$$

In the tests to be described a range of values of ρ_{dil}/ρ_h and U_{dil}/U_h was used appropriate to the high-pressure combustor being simulated. Combustor test conditions were simulated by maintaining similar Reynolds number and velocity between the experimental test rig and actual engine operation. In addition, the Reynolds number in the hot-air stream was kept sufficiently high so that turbulent mixing was assured.

Diluent-Air Hole Geometry

Several diluent-hole geometries were considered to be of interest. Round holes are simple to fabricate. Rectangular holes with the longer dimension alined in the direction of flow have better penetration characteristics than circular holes (ref. 5). Penetration can be further improved by several additional variations, for example, (1) by directing the diluent-air stream more nearly normal to the hot flow (ref. 1) or (2) by ducting the diluent-air stream by means of internal chutes (ref. 9).

Contemporary combustor diluent-air geometry is often based on circular-hole patterns; consequently, circular holes have been extensively investigated. In this investigation the primary emphasis was placed on rectangular-hole configurations and only a single representative circular-hole pattern was included. Three modifications of the rectangular-hole configuration with flush openings, with attached scoops immersed in the diluent-air stream, and with attached chutes immersed in the hot-air stream were used in four systematically varied configurations.

Sizing the round diluent holes. - A pressure drop across the holes of 4 percent of the total pressure was selected for the design point. It was assumed that frictional loss is zero, so that the 4-percent drop represents acceleration of the diluent-air jet. For the diluent-air duct and hole geometry used, a hole discharge coefficient of 0.55 was applicable (ref. 6). Using these values calculations indicated that 15.53 square inches (1.002×10^{-2} m^2) of hole area are required for the design point. The total mass flow at the design point is 4.13 pounds per second (1.88 kg/sec).

The reference diluent mass flow was selected on the basis of hypothetical engine operation. It was assumed that 35 percent of the available air would be necessary to pro-

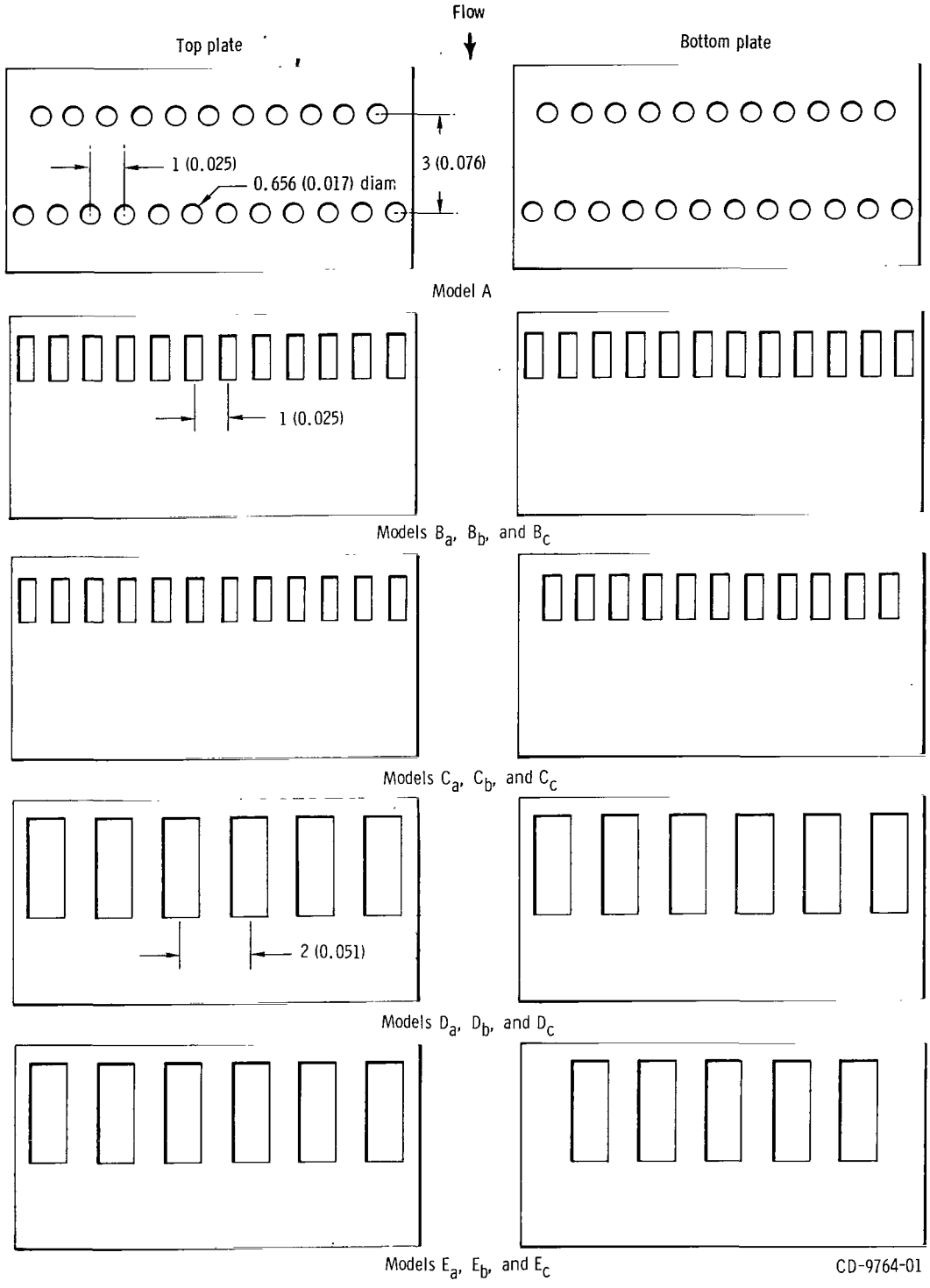

Figure 2. - Diluent-hole geometries. (All dimensions are in inches (m).)

duce the required combustor temperature rise. An empirical correlation in which combustor cooling air requirement is correlated with maximum compressor pressure ratio indicates, by extrapolation, that 35 percent of the total air will be required for cooling the combustor at a compression ratio of 20 (ref. 10). Thus, only about 30 percent of the total mass flow will be available for dilution-jet mixing at the design point.

The open circular-hole area was distributed evenly between the upper and lower dilution-zone plates. Two identical rows of holes were used on each plate.

The first row contained 11 holes spaced 1 inch (0.025 m) on centers (equal to one-half the turbine blade height). Because engine dimensions are more likely to be defined than the combustor, the spacing of the holes was referenced to the turbine blade height. The second row, 3 inches (0.076 m) downstream, contained 12 holes similarly spaced. The second row of holes was staggered with respect to the first row as shown in figure 2. The entire configuration contained 46 holes which results in an individual hole diameter of 0.656 inch (0.017 m) to maintain the calculated total open hole area.

Rectangular diluent holes. - Four basic rectangular hole patterns were selected as shown in figure 2. The four basic patterns are designated by the alphabetical description B, C, D, and E. The rectangular-slot size and type is designated by the subscripts a, b, and c for plain rectangular slots, rectangular slots with external scoops, and rectangular slots with internal chutes, respectively. A length-to-width ratio of 2.5 was chosen for the narrow plain rectangular slot based on the results of reference 5. The total hole area for each rectangular configuration was equal to the total hole area of the circular-hole configuration except for discrepancies resulting from eliminating half slots at the walls. The actual open areas of all configurations are shown in table I.

In model B_a the upper and lower dilution-hole patterns are exactly the same. Twelve rectangular holes in a single row across the duct are spaced at a distance of 1 inch (0.025 m) on centers (equal to one-half the turbine blade height). In this model the jets emerging from the upper and lower plates are opposed. Model C_a has the same hole pattern on the upper plate, but the holes in the lower plate have been offset laterally to allow opposing jets to interleave. Model D_a has a smaller number of wider slots arranged so that the jets are opposed. Model E_a has the same hole pattern on the upper plate as model D_a, but the holes in the lower plate have been offset laterally so that jets from the two plates now interleave. Each of the four rectangular-hole configurations was also tested with external scoops 1/2 inch (0.013 m) high with one guide vane (fig. 3(a)). Similar repetitive hole patterns were also used with internal chutes. The internal chutes have an immersed depth of 1 inch (0.025 m) into the hot-gas stream (fig. 3(b)). The immersed opening is a rectangular slot with a length-to-width ratio of 2, and a plate opening with a length-to-width ratio of approximately 5. Table I gives pertinent information on all models tested.

TABLE I. - SUMMARY OF EXPERIMENTAL MODEL OPEN HOLE CONFIGURATIONS

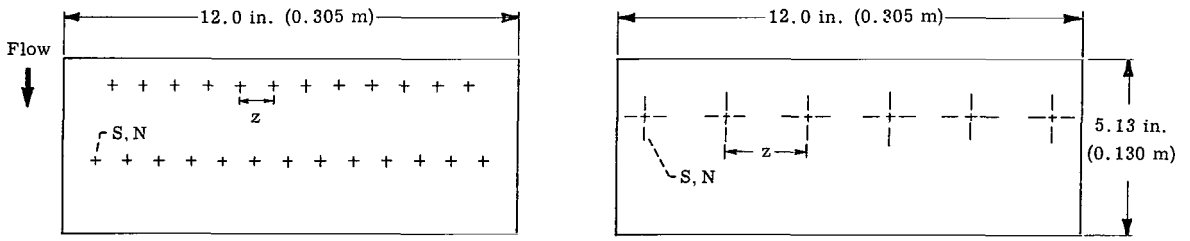

A B

Model	Sketch	Size of hole in plate, S		Number of holes in plate, N		Center-to-center hole spacing, z			Hole alinement	Hole type	Total open hole area	
		in.	m	Upper	Lower	in.	m	Percent of turbine blade height			$in.^2$	m^2
A	A	0.656 diam	0.017 diam	23	23	1	0.025	50	In line	Circular	15.53	1.002×10^{-2}
B_a	B	1.31 by 0.52	0.033 by 0.013	12	12	1	0.025	50	In line	Plain rectangular	16.47	1.063×10^{-2}
C_a	B	1.31 by 0.52	0.033 by 0.013	11	12	1	0.025	50	Staggered	Plain rectangular	15.79	1.019×10^{-2}
D_a	B	1.31 by 1.05	0.033 by 0.026	6	6	2	0.051	100	In line	Plain rectangular	16.47	1.063×10^{-2}
E_a	B	1.31 by 1.05	0.033 by 0.026	5	6	2	0.051	100	Staggered	Plain rectangular	15.13	0.976×10^{-2}
B_b	B	1.31 by 0.52	0.033 by 0.013	12	12	1	0.025	50	In line	External scoop	16.47	1.063×10^{-2}
C_b	B	1.31 by 0.52	0.033 by 0.013	11	12	1	0.025	50	Staggered	External scoop	15.79	1.019×10^{-2}
D_b	B	1.31 by 1.05	0.033 by 0.026	6	6	2	0.051	100	In line	External scoop	16.47	1.063×10^{-2}
E_b	B	1.31 by 1.05	0.033 by 0.026	5	6	2	0.051	100	Staggered	External scoop	15.13	0.976×10^{-2}
[a]B_c	B	3.00 by 0.58	0.076 by 0.015	12	12	1	0.025	50	In line	Internal chute	41.76	2.694×10^{-2}
[a]C_c	B	3.00 by 0.58	0.076 by 0.015	11	12	1	0.025	50	Staggered	Internal chute	40.02	2.582×10^{-2}
[b]D_c	B	3.00 by 1.16	0.76 by 0.029	6	6	2	0.051	100	In line	Internal chute	41.76	2.694×10^{-2}
[b]E_c	B	3.00 by 1.16	0.76 by 0.029	5	6	2	0.051	100	Staggered	Internal chute	38.28	2.470×10^{-2}

[a]Models B_c and C_c have an immersed chute which has an opening of 1.16 by 0.58 in. (0.029 by 0.015 m) in the hot stream for total areas of 16.15 and 15.47 $in.^2$ (1.042×10^{-2} and 0.998×10^{-2} m^2) for models B_c and C_c, respectively.

[b]Models D_c and E_c have an immersed chute which has an opening of 1.16 by 1.16 in. (0.029 by 0.029 m) in the hot stream for total areas of 16.15 and 14.80 $in.^2$ (1.042×10^{-2} and 0.955×10^{-2} m^2) for models D_c and C_c, respectively.

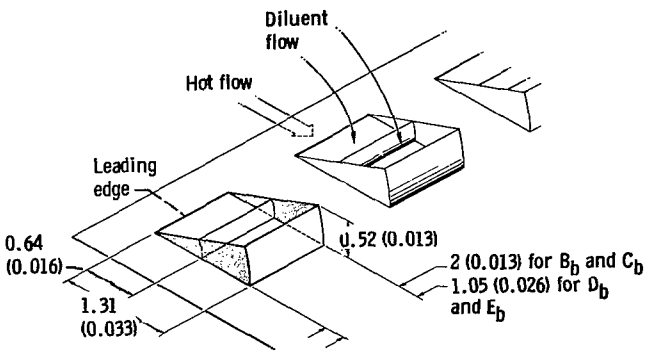

(a) Plate hole and external scoop used for models B_b, C_b, D_b, and E_b.

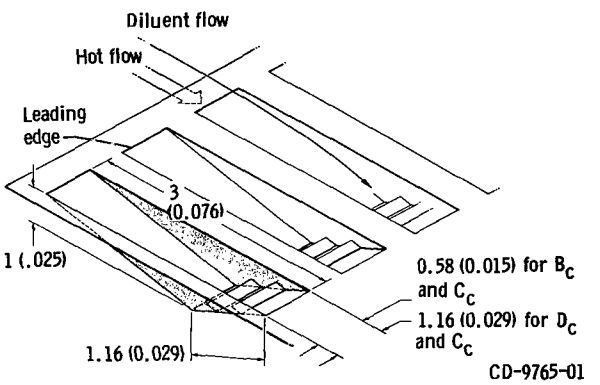

(b) Plate hole and internal chute used in models B_c, C_c, D_c, and E_c.

Figure 3. - Diluent hole geometry variation in slot size and type. (All dimensions in inches (m).)

APPARATUS

Experimental Test Facility

A diagram of the test facility is shown in figure 4. The test inlet was connected to a 140 psi (9.65×10^5 N/m^2) laboratory air supply and the test section was ducted directly to the atmosphere through a water-spray muffler. The hot stream air flow was regulated by means of a remote-controlled valve located upstream of the test section. The hot-air supply was obtained by means of a vitiating combustor and directed into a plenum chamber consisting of a swirler, plenum, and straightening section. Diluent air was regulated by manually operated valves. The diluent air was equally split to the upper and lower plates by balancing the dynamic head in the diluent passages. A plate with 70 holes, 0.75 inch (0.019 m) in diameter, was placed 15 inches (0.39 m) upstream of the dilution zone in the hot-stream passage. Calculations show that small scale turbulence from the 0.75-inch

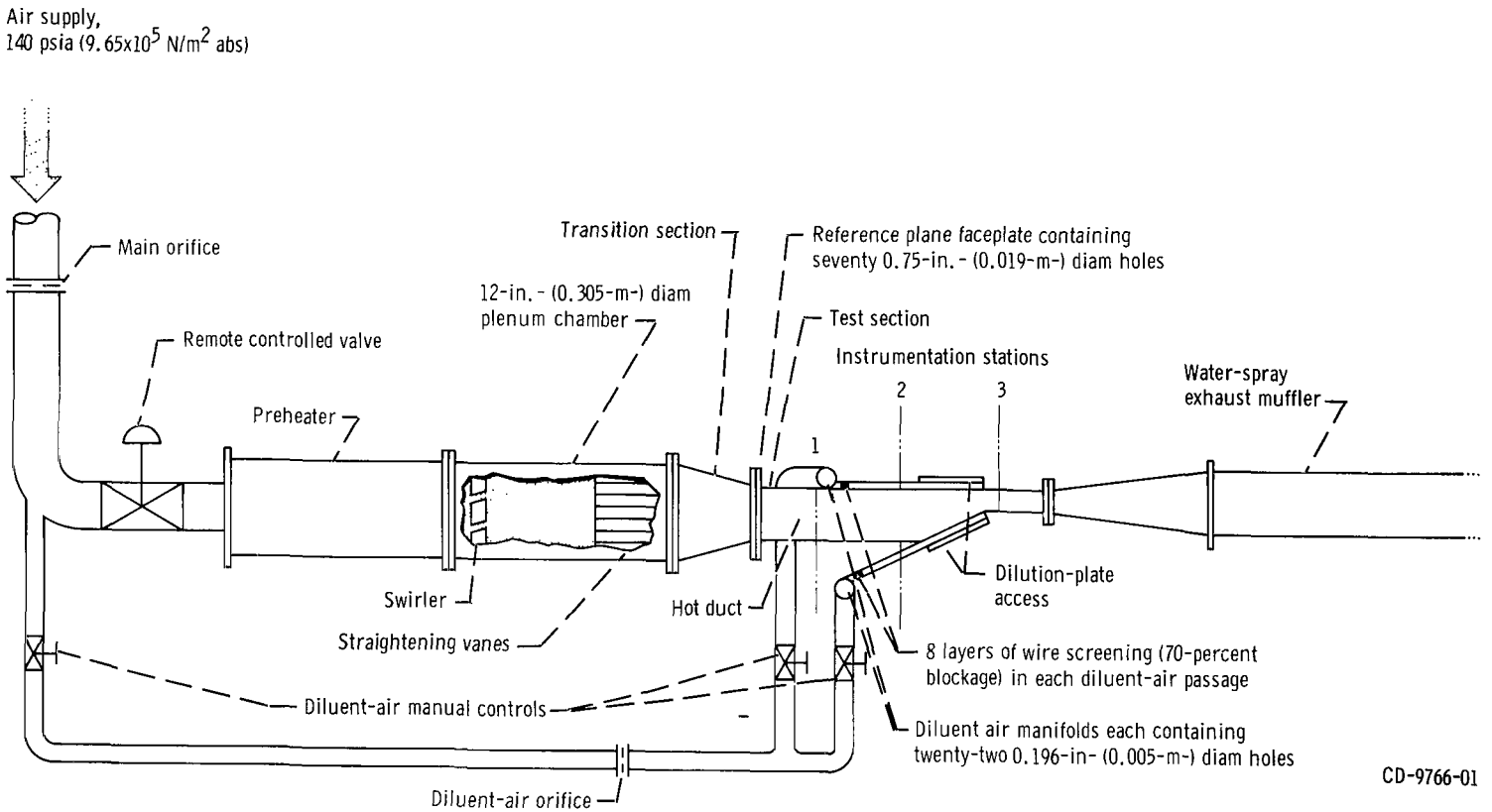

Figure 4. - Installation of experimental mixing test section.

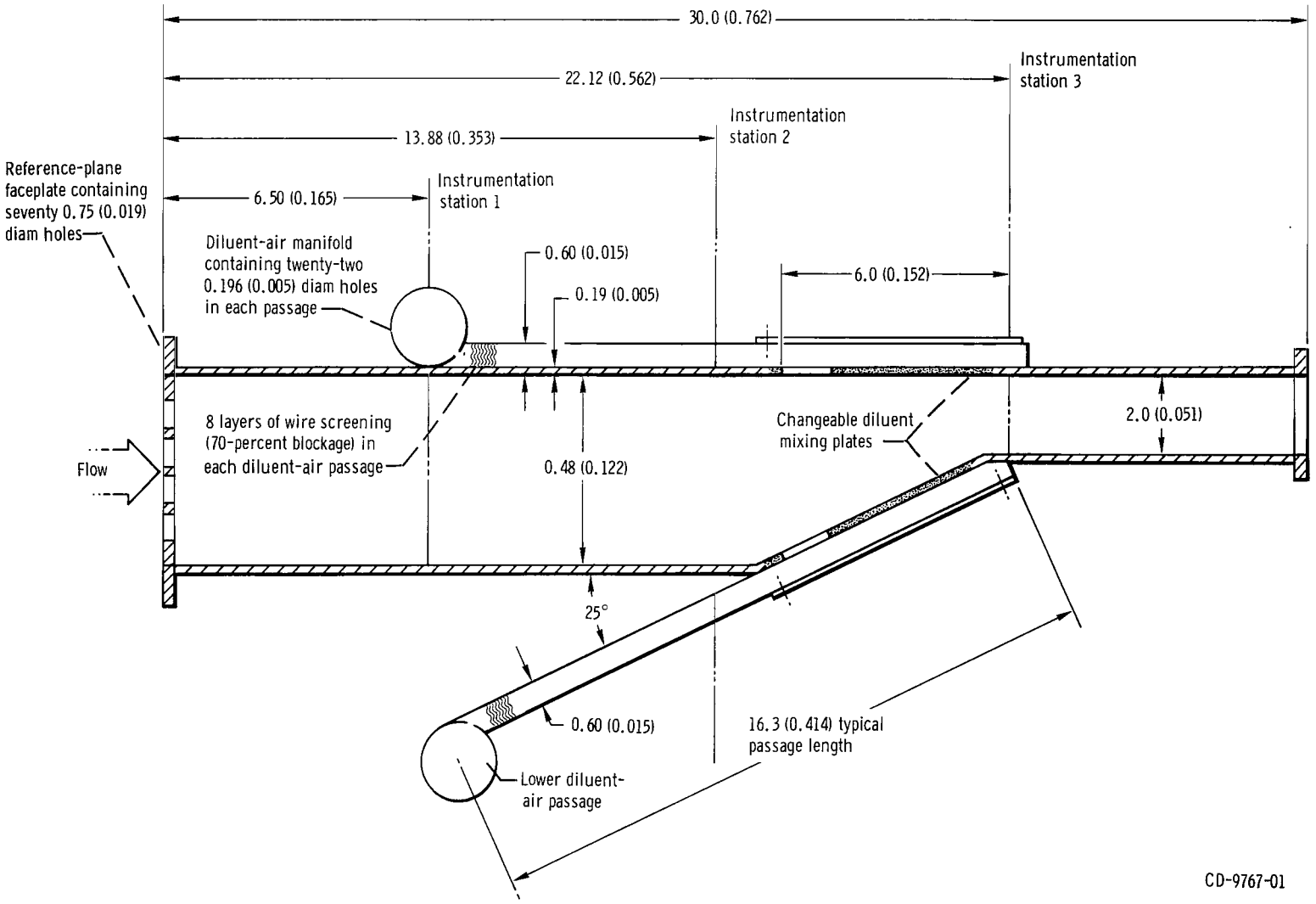

Figure 5. - Dilution zone of test section assembly. (All linear dimensions are in inches (m).)

(0.019-m) holes has dissipated prior to the dilution zone. Twenty-two evenly spaced holes, 0.196-inch (0.005 m) in diameter, were drilled into each diluent-air manifold followed immediately by eight layers of wire screening with a 70-percent blockage used to smooth out the diluent flow.

Dilution-Zone Hardware

The physical dimensions and layout of the dilution-zone hardware are shown in figure 5. The hot-stream section converges with two dilution ducts to form a dilution zone. Mixing of cold diluent stream with the hot stream is accomplished through interchangeable mixing plates 0.19-inch (0.005-m) thick as shown in figure 1(b). The distance from the leading edge of the plate containing the diluent jets to the end of the dilution mixing section, as defined by the location of the outlet instrumentation probe, is 6 inches (0.152 m) as shown in figure 5. The various mixing-plate hole configurations that were selected for testing have been presented in figures 2 and 3.

Instrumentation

Air flows were metered by sharp-edged orifices installed according to ASME specifications. Bourdon tube gages were used to measure the upstream orifice pressures, and differential pressures were obtained from strain-gage transducers. Thermocouples and pressure probes were located in the hot stream 6.50 inches (0.165 m) from the face of the punched-plate reference plane at station 1, in the diluent-stream passages 13.88 inches (0.353 m) from the reference plane at station 2, and in the exhaust section 22.13 inches (0.562 m) from the reference plane at station 3 (fig. 5). Details of the number, type, and location of instruments at the instrumentation stations are shown in figure 6. The positions of the temperature and pressure rakes at stations 1 and 2 were varied during the preliminary test runs to obtain profile data; however, all probes were fixed at the centerline of the duct during the experimental program. The outlet thermocouples and pressure tubes at station 3, which would correspond to the turbine stator plane in an actual engine, were spaced as shown in figure 6(c). All test section pressure tubes were connected to banks of manometers referenced to atmospheric pressure. A camera was used to record the manometer readings. Iron-constantan thermocouples (station 3) were connected to a self-balancing potentiometer.

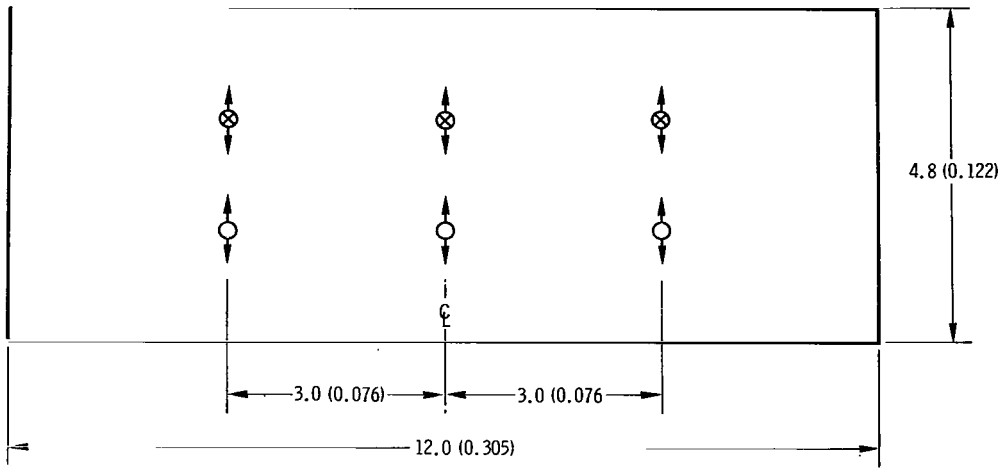

(a) Instrumentation at station 1 in hot duct, 6.50 inches (0.165 m) from reference faceplate.

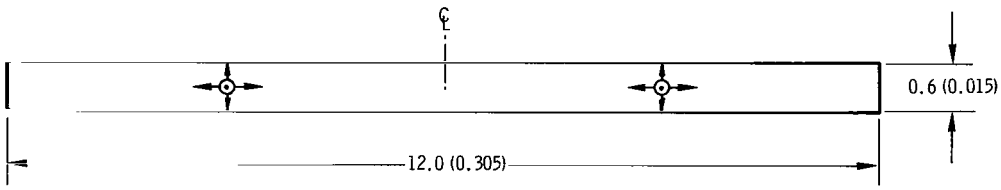

(b) Instrumentation at station 2 in upper and lower diluent ducts, 13.88 inches (0.353 m) from reference faceplate.

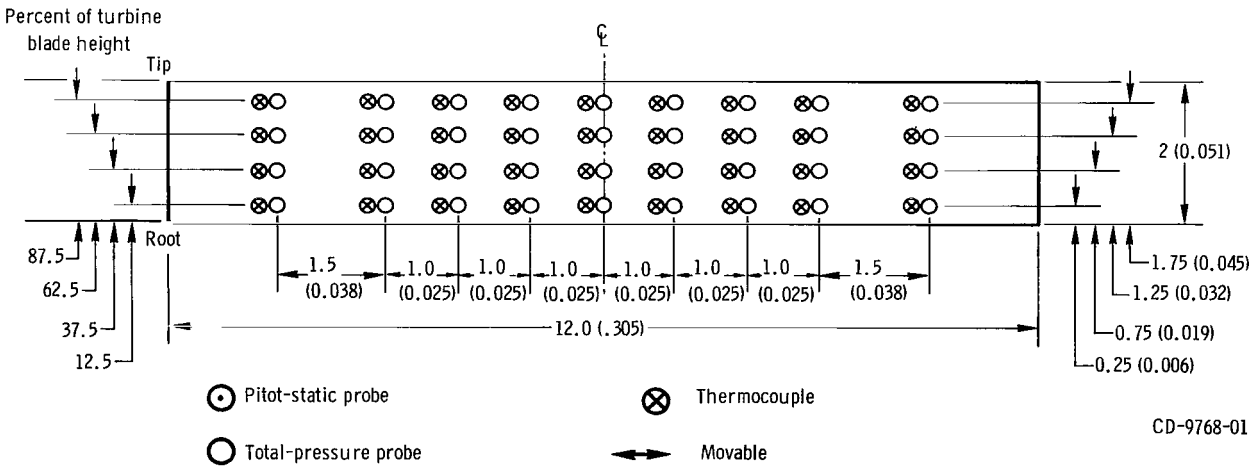

(c) Instrumentation at station 3 in exhaust duct, 22.12 inches (0.562 m) from reference faceplate.

Figure 6. - Location and details of instrumentation. (All dimensions are in inches (m).)

PROCEDURE

Test Conditions

A scaled operating condition based on Reynolds number and velocity similarity was chosen, that simulated the cruise condition for a high-compression-ratio engine. The calculated total flow was 4.13 pounds per second (1.88 kg/sec) with a hot-air temperature of 1020° R (567 K) and a diluent-air temperature at ambient temperature. As part of a parametric variation, total-mass flow rates were varied by ±25 percent and hot-stream temperatures were varied by ±15 percent based on a reference temperature of 1020° R (567 K). All test conditions are listed in table II.

TABLE II. - EXPERIMENTAL TEST CONDITIONS

Total air flow		Hot-stream temperature		Diluent-stream temperature		Ratio of diluent- to hot-stream velocity	Ratio of diluent- to hot-stream mass-flow split
lb/sec	kg/sec	°R	K	°R	K		
[a]4.13	[a]1.88	[a]1020	[a]567	[a]520	[a]289	[a]0.90	[a]30:70
4.13	1.88	1020	567	520	289	.55	20:80
4.13	1.88	1020	567	520	289	1.47	40:60
4.13	1.88	1020	567	520	289	2.20	50:50
3.10	1.41	1020	567	520	289	.90	30:70
5.16	2.34	1020	567	520	289	.90	30:70
4.13	1.88	880	489	520	289	.90	30:70
4.13	1.88	1160	644	520	289	.90	30:70

[a]Reference conditions.

Calculations

Outlet temperature profile. - The average temperature at station 3 was determined from the numerical average of all 36 iron-constantan thermocouples located as shown in figure 6(c). Radial and circumferential temperature profiles were also obtained at station 3. As previously mentioned, the upper and lower plates on the rectangular test section correspond to the outer and inner annuli in an annular combustor configuration. The distance from the lower to upper wall at station 3 will be defined herein as a radial distance. The average radial temperature distributions were obtained by averaging the readings of the nine thermocouples at each radial position and designating the lower wall

as corresponding to the root of a turbine blade. The circumferential temperature profile was obtained by averaging the readings of the four thermocouples on a given radial line at each of the nine radial lines across the duct. All temperatures were normalized with respect to the average outlet temperature, and the radial position is expressed as a percentage of the 2-inch (0.051-m) turbine blade height. The temperature profile shown in figure 7 was selected as the desired average radial profile at the turbine position.

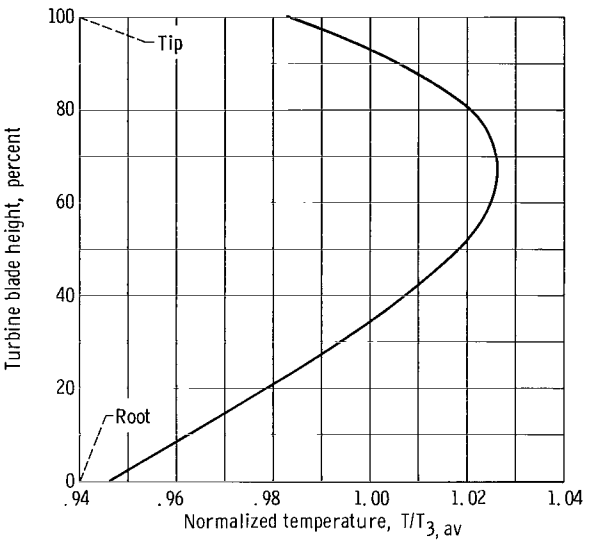

Figure 7. - Desired turbine inlet radial temperature profile.

Since localized hot zones could damage the turbine, it is common practice to also use a criterion which includes the maximum temperature experienced at the turbine position. In this study two temperature parameters were used to indicate the effectiveness of the dilution-jet mixing zone.

The first parameter is defined in the following expression:

$$\frac{T_{3,max} - T_2}{T_{3,av} - T_2} = F_s \tag{3}$$

This parameter is a measure of the maximum local temperature that might be felt by some first row turbine stator. A second parameter

$$\frac{T_{3,rad\ max} - T_2}{T_{3,av} - T_2} = F_t \tag{4}$$

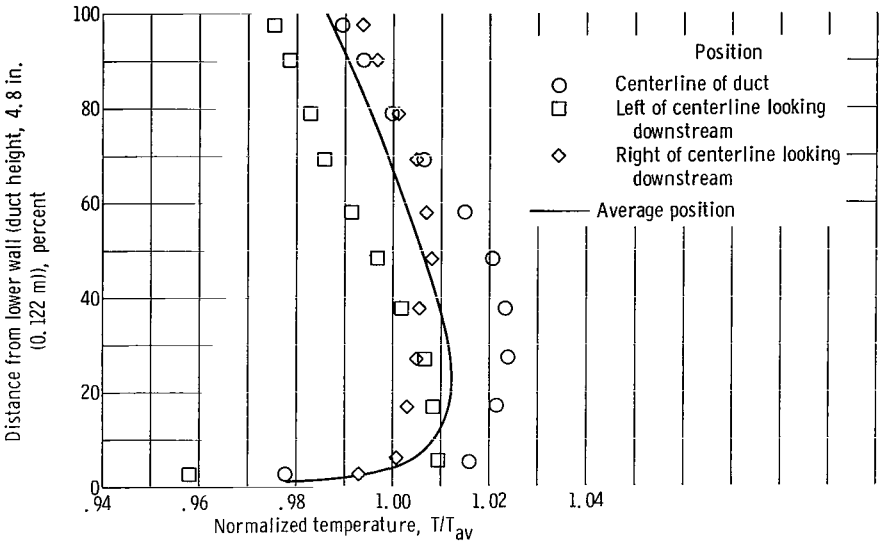

Figure 8. - Hot-stream radial-temperature profile at station 1. Standard flow conditions: hot-stream flow, 2.89 pounds per second (1.31 kg/sec); temperature, 1020° R (567 K).

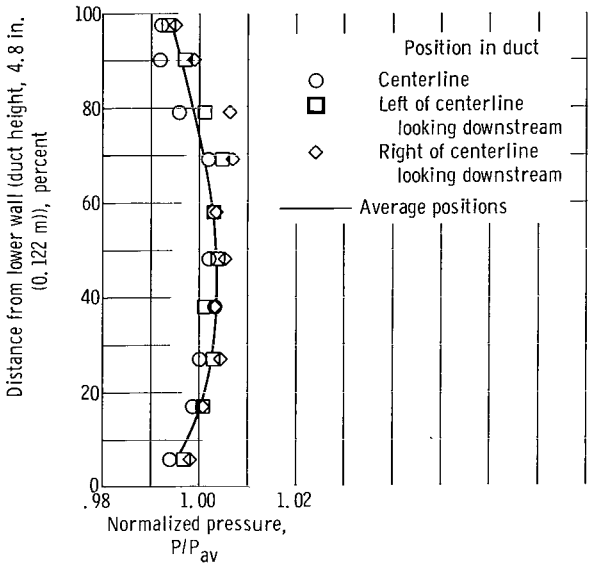

Figure 9. - Hot-stream radial-pressure profile at station 1. Standard flow conditions: hot-stream flow, 2.89 pounds per second (1.31 kg/sec); temperature, 1020° R (567 K).

was used to compare outlet profiles on the turbine rotor which is sensitive only to the circumferentially averaged temperature because of its rotation. In this case the maximum value of the average radial profile ($T_{3, rad\ max}$) is used.

Outlet total pressure profiles. - Outlet average radial-pressure profiles were obtained from the numerical average of 9 total-pressure tubes at each of the four radial positions.

Inlet Air Profiles

The hot-stream temperature and pressure profiles obtained at station 1 are shown in figures 8 and 9, respectively. The maximum variation is ±2.5 percent. The stream temperatures at station 3 without diluent flow were not obtained. It would be expected that the temperatures would be within the same temperature range as measured at station 1 because heat-transfer calculations indicated no appreciable cooling of the hot-gas stream due to the walls. The pressure profiles obtained in the diluent stream at station 2 are shown in figure 10. The maximum variation is ±1 percent.

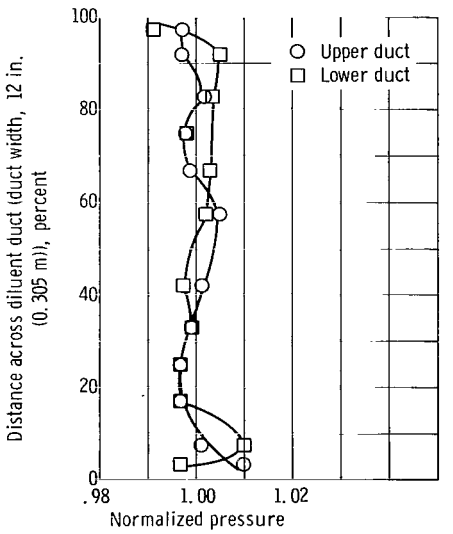

Figure 10. - Diluent-stream pressure profile at station 2. Standard flow conditions: diluent-stream air flow, 0.62 pound per second (0.28 kg/sec); temperature, ambient.

TABLE III. - EXPERIMENTAL DATA

Model number	Total mass flow, $\dot{m}_T$		Diluent-mass flow, m_2		Hot-stream temperature, T_1		Diluent-stream temperature, T_2		Average outlet temperature, T_3		Average outlet-total pressure, P_3		Percent of blade length				Temperature factor		Percent of blade length				Mach number in diluent-stream passage, M_2	Diluent-to hot-stream velocity ratio, $\frac{U_{dil}}{U_h}$	Pressure loss, $\frac{P_2 - P_3}{P_2}$, percent
													12.5	37.5	62.5	87.5			12.5	37.5	62.5	87.5			
	lb/sec	kg/sec	lb/sec	kg/sec	°R	K	°R	K	°R	K	atm	N/m²	Normalized radial temperature				F_t	F_s	Normalized radial pressure						
A_a	4.14	1.88	1.22	0.55	1008	559	518	287	878	488	1.106	1.121×10^5	0.913	1.077	1.088	0.919	1.217	1.270	0.994	1.007	1.006	0.993	0.129	0.89	2.40
	4.25	1.93	.87	.39	1002	556	523	290	905	503	1.119	1.134×10^5	.932	1.055	1.067	.947	1.158	1.433	.996	1.006	1.005	.993	.092	.52	.48
	4.16	1.89	1.66	.75	1018	565	526	292	817	454	1.106	1.121×10^5	.914	1.063	1.101	.923	1.286	1.387	.994	1.007	1.007	.990	.173	1.33	5.41
	4.18	1.90	2.10	.95	1016	564	527	292	764	425	1.100	1.115×10^5	.945	1.053	1.069	.931	1.224	1.371	.995	1.007	1.009	.990	.216	2.00	8.45
	4.56	2.07	1.57	.71	1019	566	522	290	852	474	1.135	1.150×10^5	.914	1.062	1.097	.926	1.255	1.338	.993	1.008	1.007	.992	.161	1.06	4.14
	3.12	1.42	.91	.41	1008	559	524	291	872	485	1.054	1.068×10^5	.913	1.056	1.095	.934	1.240	1.283	.996	1.004	1.004	.996	.101	.83	1.10
	4.20	1.91	1.25	.57	1147	637	524	291	976	543	1.127	1.142×10^5	.904	1.088	1.101	.907	1.217	1.273	.994	1.008	1.007	.992	.128	.75	2.36
	4.15	1.88	1.23	.56	882	490	521	289	779	433	1.091	1.105×10^5	.928	1.067	1.073	.933	1.224	1.290	.996	1.004	1.006	.995	.130	.97	2.40
B_a	4.10	1.86	1.21	0.55	1008	559	528	293	872	485	1.114	1.128×10^5	0.943	1.061	1.075	0.921	1.189	1.288	0.999	1.003	1.002	0.995	0.128	0.85	2.27
	4.21	1.91	.80	.36	1019	566	536	297	932	518	1.133	1.148×10^5	.959	1.049	1.061	.932	1.142	1.170	.999	1.003	1.002	.995	.085	.48	.30
	4.07	1.85	1.65	.75	1012	562	529	294	825	459	1.104	1.119×10^5	.949	1.069	1.062	.919	1.192	1.407	.999	1.002	1.003	.995	.173	1.36	4.64
	4.27	1.94	2.17	.99	1015	563	528	293	770	428	1.106	1.121×10^5	.973	1.053	1.042	.930	1.169	1.331	.999	1.006	1.004	.993	.224	1.96	7.98
	4.64	2.11	1.51	.69	1019	566	530	294	862	479	1.153	1.168×10^5	.946	1.070	1.073	.909	1.189	1.317	.997	1.004	1.004	.994	.154	.97	3.42
	3.15	1.43	.89	.40	1024	568	536	297	888	494	-----	---------	.939	1.058	1.078	.926	1.194	1.264	-----	-----	-----	-----	.100	.81	----
	4.07	1.85	1.22	.55	1135	630	528	293	963	535	1.125	1.140×10^5	.934	1.070	1.085	.910	1.188	1.276	.998	1.004	1.003	.994	.128	.77	2.31
	4.15	1.88	1.24	.56	882	490	528	293	780	434	1.101	1.116×10^5	.948	1.050	1.067	.938	1.177	1.294	.999	1.003	1.002	.995	.133	.99	2.55
C_a	4.14	1.88	1.21	0.55	1020	566	511	284	873	485	1.111	1.126×10^5	0.942	1.061	1.073	0.922	1.181	1.288	0.999	1.004	1.004	.995	0.126	0.81	2.33
	4.18	1.90	.82	.37	1015	563	511	284	916	509	1.119	1.134×10^5	.959	1.049	1.061	.931	1.141	1.166	.999	1.003	1.003	.995	.086	.49	.48
	4.24	1.92	1.64	.74	1012	562	513	285	822	457	1.110	1.125×10^5	.948	1.066	1.066	.921	1.178	1.333	.999	1.005	1.003	.994	.169	1.23	4.51
	4.12	1.87	2.10	.95	1015	563	515	286	766	426	1.099	1.114×10^5	.984	1.064	1.014	.937	1.200	1.302	.997	1.006	1.005	.992	.214	1.95	7.66
	4.70	2.13	1.51	.69	1022	567	508	282	838	466	1.149	1.164×10^5	.945	1.070	1.068	.916	1.184	1.364	.999	1.005	1.004	.993	.151	.91	3.43
	3.09	1.40	.86	.39	1019	566	506	281	873	485	1.054	1.068×10^5	.944	1.067	1.070	.916	1.171	1.294	.999	1.003	1.002	.997	.094	.76	1.21
	4.09	1.86	1.21	.55	1144	635	512	284	965	537	1.125	1.140×10^5	.936	1.068	1.083	.911	1.179	1.285	.998	1.004	1.004	.994	.125	.74	2.19
	4.14	1.88	1.21	.55	874	485	511	284	766	426	1.096	1.111×10^5	.948	1.044	1.065	.945	1.202	1.300	.999	1.003	1.002	.995	.128	.95	2.36
D_a	4.16	1.89	1.18	0.54	1026	569	513	285	872	485	1.113	1.128×10^5	0.971	1.036	1.046	0.949	1.113	1.333	1.001	1.001	1.001	0.997	0.123	0.77	2.38
	4.23	1.92	.82	.37	1007	559	520	289	904	503	1.121	1.136×10^5	.960	1.035	1.060	.946	1.142	1.211	.999	1.002	1.002	.997	.087	.49	.66
	4.21	1.91	1.71	.78	1020	566	527	292	820	456	1.106	1.121×10^5	1.009	1.024	.995	.970	1.068	1.290	1.001	1.001	.999	1.000	.178	1.34	5.52
	4.22	1.92	2.10	.95	1017	564	539	299	780	434	1.106	1.121×10^5	1.040	1.010	.970	.999	1.128	1.230	.999	1.000	.999	1.002	.218	1.93	8.50
	4.49	2.04	1.51	.69	1016	564	542	301	847	471	1.138	1.153×10^5	.993	1.031	1.025	.953	1.084	1.347	1.002	1.001	.999	.999	.157	1.03	4.23
	3.11	1.41	.90	.41	1017	564	543	301	870	484	1.058	1.072×10^5	.974	1.033	1.039	.952	1.101	1.334	1.000	1.000	.999	.999	.102	.85	1.58
	4.08	1.85	1.07	.49	1149	638	515	286	973	541	1.132	1.147×10^5	.968	1.042	1.056	.934	1.119	1.316	1.000	1.001	1.001	.996	.110	.62	2.06
	4.08	1.85	1.07	.49	881	489	514	285	772	429	1.107	1.122×10^5	.983	1.028	1.034	.959	1.103	1.340	1 002	.999	1.001	.999	.112	.80	1.80

E_a	4.12	1.87	1.21	0.55	1011	561	528	293	865	481	1.115	1.130×10^5	0.975	1.022	1.037	0.965	1.095	1.252	1.001	1.001	1.001	0.998	0.127	0.84	2.90
	4.18	1.90	.82	.37	1007	559	531	295	909	505	1.126	1.141×10^5	.954	1.027	1.053	.965	1.126	1.271	.999	1.002	1.002	.997	.087	.50	.78
	4.07	1.85	1.64	.74	1018	565	532	295	818	455	1.106	1.121×10^5	1.022	1.008	.987	.987	1.062	1.250	1.001	1.000	.999	1.001	.172	1.34	5.90
	4.17	1.89	2.15	.98	1034	574	538	299	764	425	1.106	1.121×10^5	1.033	.998	.981	.992	1.109	1.243	.999	.998	.997	1.005	.221	2.02	9.56
	4.56	2.07	1.53	.69	1012	562	541	300	842	468	1.145	1.160×10^5	.988	1.021	1.018	.973	1.058	1.266	1.003	1.001	1.001	.996	.158	1.04	4.86
	3.20	1.45	.90	.41	1026	569	540	300	874	486	1.063	1.077×10^5	.971	1.021	.923	.970	1.097	1.290	1.001	1.001	1.000	.999	.101	.81	1.76
	4.15	1.88	1.21	.55	1149	638	528	293	960	534	1.129	1.144×10^5	.966	1.027	1.054	.954	1.120	1.278	1.001	1.001	1.002	.997	.126	.73	2.87
	4.14	1.88	1.21	.55	878	487	528	293	770	428	1.100	1.115×10^5	.981	1.016	1.029	.977	1.091	12.89	1.001	1.001	1.000	.998	.130	.96	3.06
B_b	4.15	1.88	1.25	0.57	1019	566	507	281	871	484	1.102	1.117×10^5	0.943	1.063	1.079	0.915	1.193	1.305	0.998	1.004	1.004	0.993	0.130	0.82	2.70
	4.23	1.92	.80	.36	1014	563	507	281	919	511	1.115	1.130×10^5	.959	1.047	1.062	.932	1.141	1.163	.999	1.004	1.003	.995	.084	.46	.49
	4.16	1.89	1.65	.75	1012	562	506	281	816	448	1.096	1.111×10^5	.948	1.059	1.071	.919	1.192	1,384	.998	1.006	1.003	.993	.170	1.21	5.18
	4.14	1.88	2.12	.96	1018	565	507	281	774	430	1.084	1.098×10^5	.963	1.049	1.044	.945	1.147	1.506	.997	1.007	1.005	.992	.216	1.85	8.34
	4.58	2.08	1.61	.73	1024	568	507	281	848	471	1.130	1.145×10^5	.936	1.075	1.078	.911	1.198	1.492	.998	1.006	1.004	.992	.161	1.00	4.54
	3.09	1.40	.90	.41	1023	568	506	281	878	488	1.051	1.065×10^5	.940	1.059	1.078	.924	1.190	1.294	.999	1.003	1.002	.996	.099	.79	1.53
	4.02	1.83	1.23	.56	1142	634	506	281	952	529	1.107	1.122×10^5	.935	1.069	1.089	.908	1.194	1.265	.998	1.004	1.004	.993	.127	.74	2.63
	4.16	1.89	1.26	.57	886	492	506	281	779	433	1.089	1.103×10^5	.951	1.040	1.064	.943	1.195	1.298	.999	1.004	1.003	.994	.132	.94	2.91
C_b	4.12	1.87	1.24	0.56	1008	559	519	288	848	471	1.112	1.127×10^5	0.948	1.062	1.066	0.923	1.173	1.324	0.998	1.004	1.003	0.994	0.130	0.86	2.85
	4.20	1.91	.79	.36	1007	559	517	287	907	504	1.127	1.142×10^5	.958	1.047	1.061	.933	1.143	1.182	.998	1.003	1.003	.995	.082	.47	.12
	4.16	1.89	1.65	.75	1014	563	512	284	808	449	1.106	1.121×10^5	.962	1.060	1.046	.932	1.169	1.386	.997	1.004	1.004	.994	.169	1.25	5.35
	4.18	1.90	2.09	.95	1023	568	511	284	764	425	1.098	1.113×10^5	.979	1.042	1.005	.972	1.130	1.228	.994	1.006	1.005	.994	.211	1.81	8.30
	4.74	2.15	1.53	.69	1017	564	510	283	839	466	1.138	1.153×10^5	.949	1.069	1.062	.920	1.180	1.381	.997	1.005	1.004	.994	.154	.91	4.23
	2.58	1.17	.89	.41	1024	568	507	281	870	484	1.050	1.064×10^5	.938	1.059	1.071	.932	1.175	1.297	.999	1.003	1.003	.997	.098	1.02	1.66
	4.14	1.88	1.22	.55	1142	634	522	290	949	528	1.127	1.142×10^5	.939	1.070	1.078	.913	1.174	1.322	.998	1.004	1.004	.995	.126	.74	2.64
	4.21	1.91	1.24	.56	876	486	520	289	763	424	1.104	1.119×10^5	.947	1.043	1.062	.946	1.196	1.321	.998	1.003	1.003	.995	.131	.96	2.87
D_b	4.14	1.88	1.20	0.54	1020	566	508	282	865	481	1.112	1.127×10^5	0.993	1.022	1.018	0.967	1.054	1.335	1.001	1.001	1.001	0.998	0.124	0.79	2.79
	4.06	1.84	.79	.36	1010	561	509	282	912	507	1.112	1.127×10^5	.984	1.023	1.043	.950	1.099	1.203	.993	1.001	1.002	.997	.083	.48	.61
	4.09	1.86	1.57	.71	1022	567	509	282	826	459	1.103	1.118×10^5	1.030	1.013	.967	.987	1.081	1.260	1.003	1.000	.997	1.001	.162	1.18	5.09
	4.21	1.91	2.16	.98	1007	559	509	282	749	416	1.096	1.111×10^5	1.032	.994	.977	.997	1.103	1.211	.999	.999	.997	1.002	.215	1.94	9.18
	4.79	2.17	1.56	.71	1011	561	510	283	832	463	1.152	1.167×10^5	1.006	1.013	.993	.978	1.054	1.344	1.002	1.000	.998	.999	.154	.92	4.40
	3.16	1.43	.90	.41	1021	567	509	282	862	479	1.057	1.071×10^5	.998	1.021	1.011	.970	1.052	1.323	1.001	1.001	.999	.999	.099	.78	1.77
	4.10	1.86	1.17	.53	1142	634	510	283	952	529	1.119	1.134×10^5	.980	1.029	1.031	.961	1.067	1.322	1.001	1.001	1.001	.998	.120	.70	2.61
	3.72	1.69	1.19	.54	877	487	509	282	763	424	1.096	1.111×10^5	.992	1.013	1.010	.983	1.041	1.354	1.001	1.000	.999	.999	.125	1.06	2.83
E_b	4.18	1.90	1.25	0.57	1015	563	508	282	861	479	1.115	1.130×10^5	0.990	1.003	1.028	0.978	1.070	1.229	1.002	0.999	1.001	0.999	0.129	0.82	3.44
	4.16	1.89	.81	.37	1013	562	510	283	916	509	1.123	1.138×10^5	.976	1.012	1.054	.956	1.123	1.168	.999	1.001	1.002	.996	.092	.52	.91
	4.19	1.90	1.66	.75	1014	563	510	283	811	451	1.110	1.125×10^5	1.028	.990	.973	1.006	1.078	1.212	1.002	.999	.999	1.002	.170	1.25	6.30
	4.20	1.91	2.14	.97	1011	561	510	283	752	418	1.111	1.126×10^5	1.014	1.001	.992	.995	1.043	1.289	1.003	.996	.995	1.006	.213	1.90	9.88
	4.70	2.13	1.56	.71	1019	566	508	282	849	472	1.157	1.172×10^5	1.004	1.004	1.006	.987	1.015	1.241	1.002	.999	.999	.999	.156	.94	4.98
	3.12	1.42	.91	.41	1014	563	507	281	857	476	1.053	1.067×10^5	.985	1.002	1.032	.979	1.099	1.249	1.001	.999	1.001	.999	.099	.80	2.09
	4.16	1.89	1.25	.57	1152	639	508	282	952	529	1.127	1.142×10^5	.985	1.007	1.038	.967	1.083	1.234	1.001	.999	1.001	.999	.128	.73	3.29
	4.15	1.88	1.25	.57	878	487	508	282	766	426	1.097	1.112×10^5	.987	.999	1.021	.995	1.064	1.236	1.002	.999	1.000	.999	.131	.91	3.49

TABLE III. - Concluded. EXPERIMENTAL DATA

Model number	Total mass flow, m_T		Diluent-mass flow, m_2		Hot-stream temperature, T_1		Diluent-stream temperature, T_2		Average outlet temperature, T_3		Average outlet-total pressure, P_3		Percent of blade length				Temperature factor		Percent of blade length				Mach number in diluent-stream passage, M_2	Diluent-to hot-stream velocity ratio, $\frac{U_{dil}}{U_h}$	Pressure loss, $\frac{P_2 - P_3}{P_2}$, percent
													12.5	37.5	62.5	87.5			12.5	37.5	62.5	87.5			
	lb/sec	kg/sec	lb/sec	kg/sec	°R	K	°R	K	°R	K	atm	N/m^2	Normalized radial temperature				F_t	F_s	Normalized radial pressure						
B_c	4.13	1.88	1.24	0.56	1002	556	524	291	827	460	1.099	1.114×10^5	0.940	1.018	1.043	1.001	1.135	1.231	0.995	1.008	0.996	1.002	0.134	.89	----
	4.09	1.86	.80	.36	1010	561	529	294	896	498	1.111	1.126×10^5	.954	.998	1.033	1.015	1.078	1.141	.994	1.002	.999	1.003	.089	.52	----
	4.11	1.87	1.66	.75	1009	560	529	294	794	441	1.089	1.103×10^5	.935	1.017	1.052	1.000	1.153	1.284	.998	1.010	.997	.996	.179	1.39	2.91
	4.15	1.88	2.00	.91	1020	566	527	292	762	424	1.089	1.103×10^5	.948	1.006	1.054	.994	1.174	1.318	.998	1.009	1.007	.992	.212	1.85	5.43
	4.55	2.07	1.51	.69	1025	569	527	292	826	460	1.127	1.142×10^5	.934	.922	1.038	1.005	1.140	1.229	.995	1.010	.993	1.002	.159	1.02	1.19
	3.14	1.43	.92	.42	1014	563	500	278	854	475	1.053	1.067×10^5	.934	1.013	1.040	1.014	1.100	1.174	.994	1.003	.994	1.000	.101	.82	.26
	4.11	1.87	1.23	.56	1136	630	525	291	932	518	1.114	1.129×10^5	.931	1.012	1.044	1.012	1.101	1.194	.993	1.007	.994	1.004	.133	.79	----
	4.08	1.85	1.22	.55	890	494	525	291	767	426	1.085	1.099×10^5	.937	1.010	1.039	1.010	1.116	1.198	.996	1.008	.996	1.002	.134	1.01	.25
C_c	4.14	1.88	1.22	0.55	1019	566	536	297	840	467	1.105	1.120×10^5	0.946	1.025	1.000	1.030	1.079	1.158	0.994	1.006	0.995	1.005	0.139	0.87	----
	4.15	1.88	.81	.37	1007	559	534	296	882	490	1.115	1.130×10^5	.973	1.016	1.005	1.008	1.039	1.165	.996	1.004	.994	1.005	.094	.52	----
	4.13	1.88	1.62	.74	1018	565	525	291	803	446	1.099	1.114×10^5	.944	1.027	1.001	1.027	1.079	1.219	.997	1.009	.996	.999	.182	1.21	1.23
	4.14	1.88	2.08	.94	1016	564	519	289	766	426	1.099	1.114×10^5	.948	1.016	1.021	1.014	1.066	1.352	.992	1.003	.997	.989	.232	2.03	3.23
	4.63	2.10	1.54	.70	1019	566	510	283	831	462	1.133	1.148×10^5	.943	1.029	.996	1.034	1.089	1.182	.995	1.008	.993	1.004	.169	.99	----
	3.14	1.43	.92	.42	1025	569	506	286	857	476	1.053	1.067×10^5	.943	1.027	.999	1.033	1.082	1.176	.997	1.000	.995	1.002	.104	.82	----
	4.09	1.86	1.20	.54	1134	629	535	297	922	513	1.117	1.132×10^5	.934	1.018	1.007	1.041	1.095	1.221	.994	1.005	.994	1.006	.137	.79	----
	4.15	1.88	1.22	.55	888	493	535	297	765	425	1.094	1.108×10^5	.937	1.012	1.006	1.046	1.141	1.249	.995	1.006	.994	1.004	.140	1.00	----
D_c	4.13	1.88	1.23	0.56	1015	563	517	287	852	474	1.109	1.124×10^5	0.992	0.983	0.979	1.048	1.124	1.347	1.002	1.000	0.988	1.010	0.132	0.86	----
	4.18	1.90	.81	.37	1023	568	505	280	898	499	1.125	1.140×10^5	.983	.985	.997	1.036	1.084	1.272	1.002	1.002	.988	1.008	.087	.48	----
	4.17	1.89	1.64	.74	1006	558	511	284	816	454	1.106	1.121×10^5	.996	1.006	.968	1.030	1.081	1.292	1.004	1.003	.988	1.004	.173	1.30	1.75
	4.16	1.89	2.04	.93	1012	562	515	286	788	438	1.100	1.115×10^5	.972	1.013	.989	1.024	1.071	1.455	1.004	1.004	.994	.998	.213	1.90	2.43
	4.62	2.10	1.50	.68	1023	568	518	287	846	470	1.143	1.158×10^5	1.001	.988	.973	1.040	1.105	1.351	1.005	1.000	.985	1.010	.156	.97	.12
	3.17	1.44	.89	.40	1020	566	526	292	864	480	1.061	1.075×10^5	.996	.988	.971	1.048	1.122	1.320	1.003	1.000	.990	1.006	.100	.81	----
	4.17	1.89	1.23	.56	1133	629	524	291	942	524	1.125	1.140×10^5	.989	.977	.979	1.054	1.121	1.363	1.004	.999	.987	1.011	.131	.78	----
	4.07	1.85	1.21	.55	874	485	524	291	770	428	1.093	1.107×10^5	.978	.992	.983	1.049	1.153	1.365	1.003	.999	.988	1.009	.132	1.01	----
E_c	4.12	1.87	1.21	0.55	1012	562	516	286	868	483	1.100	1.115×10^5	0.985	0.986	0.984	1.047	1.106	1.252	1.002	0.997	0.993	1.009	0.130	0.84	----
	4.09	1.86	.80	.36	1016	564	512	284	905	503	1.110	1.125×10^5	.967	.975	1.022	1.032	1.075	1.220	1.004	.996	.993	1.008	.087	.49	----
	4.09	1.86	1.63	.74	1011	561	510	283	825	459	1.099	1.114×10^5	.991	1.004	.954	1.052	1.139	1.269	1.000	.999	.996	1.005	.173	1.31	1.58
	4.13	1.88	2.08	.94	1014	563	533	296	748	416	1.104	1.119×10^5	.997	.975	.990	1.043	1.130	1.673	.999	.999	1.002	1.001	.221	2.02	4.64
	4.63	2.10	1.51	.69	1022	567	536	297	864	480	1.150	1.165×10^5	.987	.985	.976	1.052	1.133	1.289	1.002	.997	.990	1.011	.159	1.01	.19
	3.16	1.43	.89	.40	1015	563	533	296	882	490	1.060	1.074×10^5	.969	.979	1.004	1.045	1.112	1.275	1.001	.998	.995	1.006	.101	.82	----
	4.10	1.86	1.22	.55	1141	633	517	287	954	530	1.117	1.132×10^5	.982	.975	.989	1.052	1.115	1.272	1.001	.996	.992	1.010	.131	.77	----
	4.07	1.85	1.21	.55	876	486	516	286	776	431	1.087	1.101×10^5	.973	.993	.987	1.046	1.137	1.266	1.002	.998	.993	1.008	.132	.98	----

RESULTS AND DISCUSSION

The experimental data obtained in the investigation of the hole configurations for the dilution-jet mixing study are presented in table III.

Effect of Diluent- to Hot-Stream Velocity Ratio on Temperature Profile

The radial-temperature profiles for 13 experimental dilution patterns at four diluent- to hot-stream velocity ratios at a constant total air flow and inlet temperature are presented in figure 11.

Circular hole configuration (model A). - The effect of four diluent- to hot-stream velocity ratios for the circular hole geometry is shown in figure 11(a). As previously discussed the depth of penetration depends on the velocity ratio of the diluent to the hot stream (eq. (2)), and, as this ratio is increased, penetration should be improved. In these tests it was not possible to vary the velocity ratio for a given test condition without changing geometry; therefore, the velocity was varied by a redistribution of the total mass flow. When the velocity ratio is varied in this manner, mixing requirements change. For example, when the diluent- to hot-stream velocity ratio is 0.52, 80 percent of the mass flow is in the hot-gas stream and 20 percent remains to be mixed; when the velocity ratio is 0.89, 30 percent remains to be mixed. Thus, mixing requirements increase as velocity ratio increases.

It is possible with extremely poor mixing that the maximum average temperature at some radial position could equal that of the hot stream. In this case, the maximum value that the normalized temperature ratio could attain is dependent on the hot-stream temperature (T_1) and the equilibrium exit temperature ($T_{3,av}$). Values of $T_1/T_{3,av}$ are tabulated in table IV for the range of velocity ratios investigated. The maximum normalized temperature ratio T_1/T_3 increases for increasing velocity ratio, reflecting the increased mixing requirements.

To gain an insight as to the degree of mixing experienced, the temperature difference between the hot stream and the maximum value of the temperature determined from the actual radial profile was compared with the difference between the hot stream and the ideal average temperature as determined from thermodynamic and turbine blade stress considerations. The values of

$$\frac{T_1 - T_{3,\text{rad max}}}{T_1 - T_{3,\text{id}}}$$

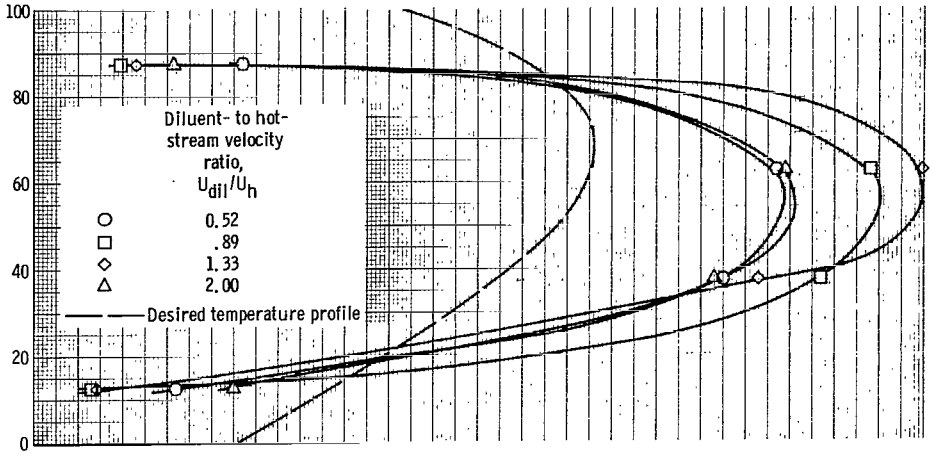

(a) Model A (circular holes).

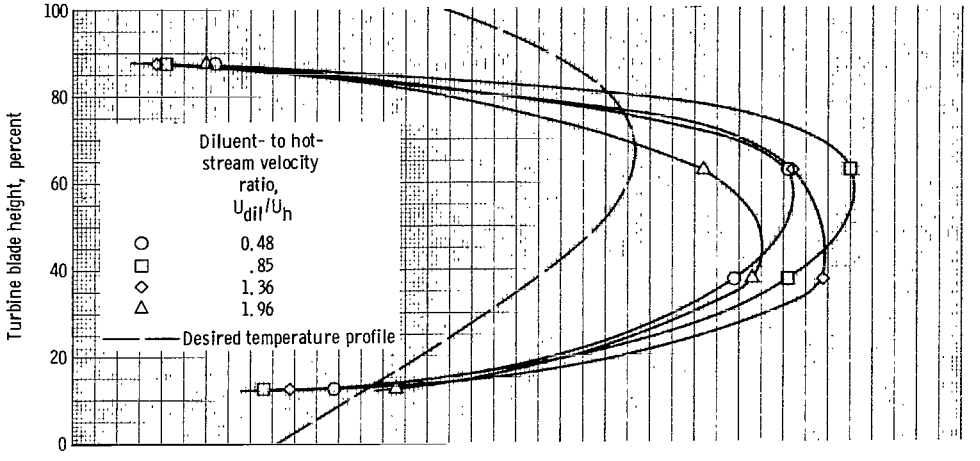

(b) Model B_a (opposing rectangular holes in-line, half turbine blade height spacing).

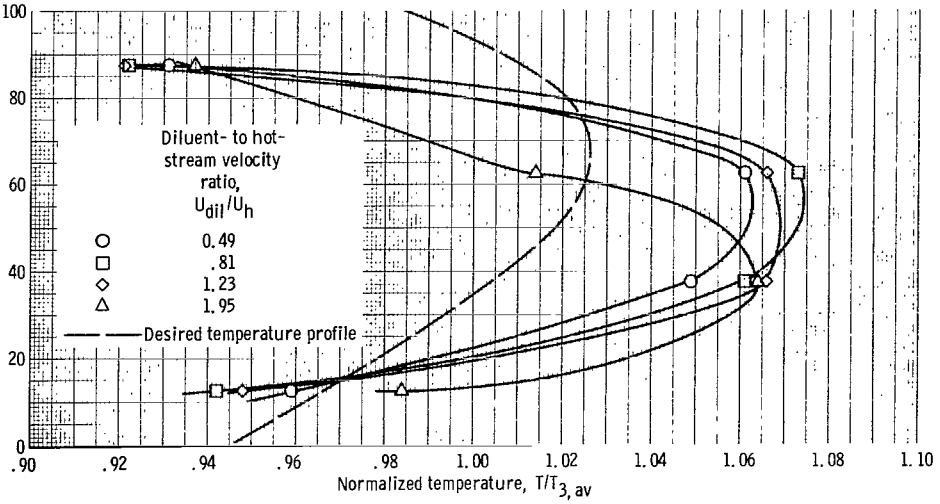

(c) Model C_a (opposing rectangular holes staggered, half turbine blade height spacing).

Figure 11. - Turbine inlet radial temperature profiles at station 3. Standard flow conditions: total air flow, 4.13 pounds per second (1.88 kg/sec); hot-stream temperature, 1020° R (567 K); diluent-stream temperature, ambient.

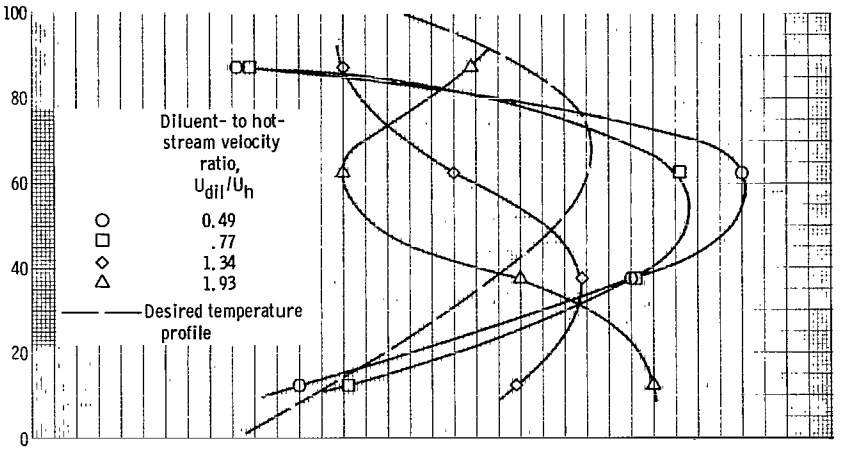

(d) Model D_a (opposing rectangular holes in-line, turbine blade height spacing).

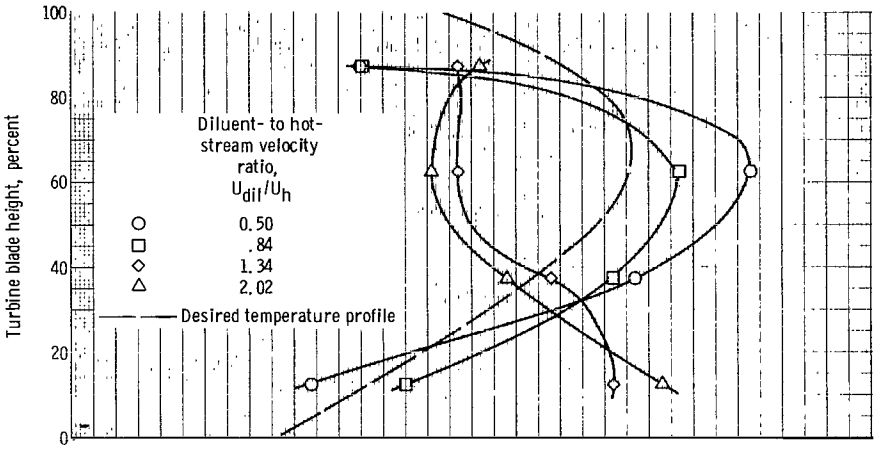

(e) Model E_a (opposing rectangular holes staggered, turbine blade height spacing).

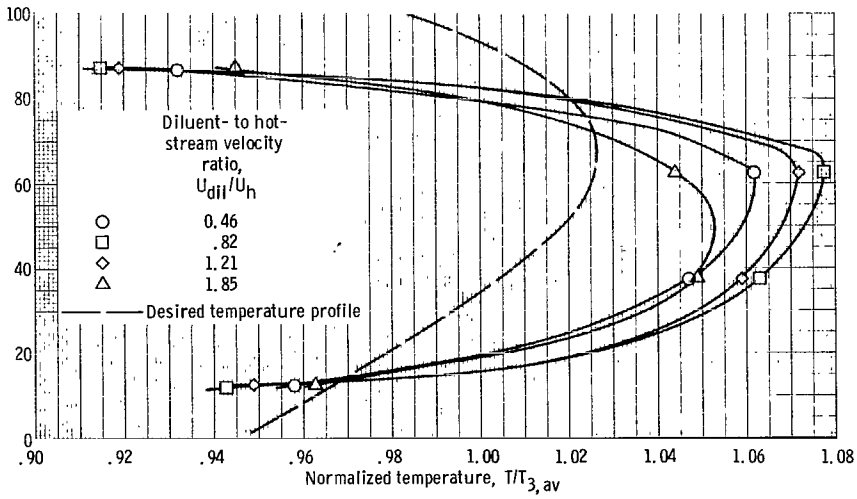

(f) Model B_b (opposing external scoops in-line, half turbine blade height spacing).

Figure 11. - Continued.

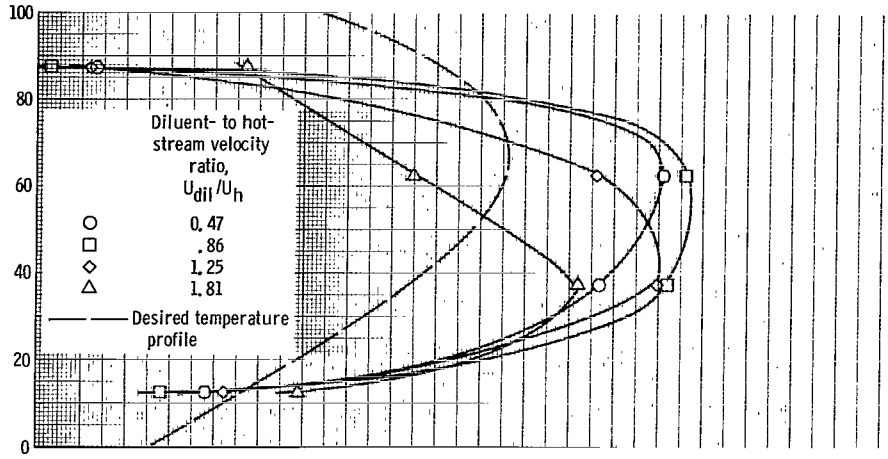

(g) Model C_b (opposing external scoops staggered, half turbine blade height spacing).

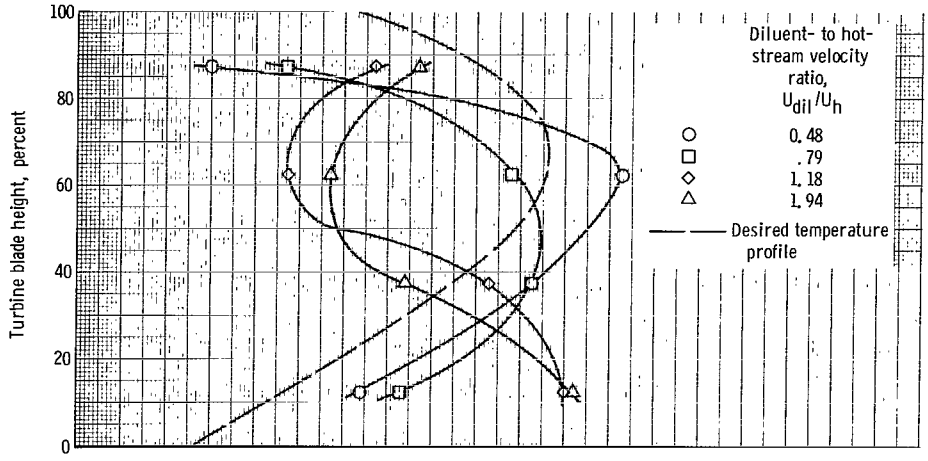

(h) Model D_b (opposing external scoops in-line, turbine blade height spacing).

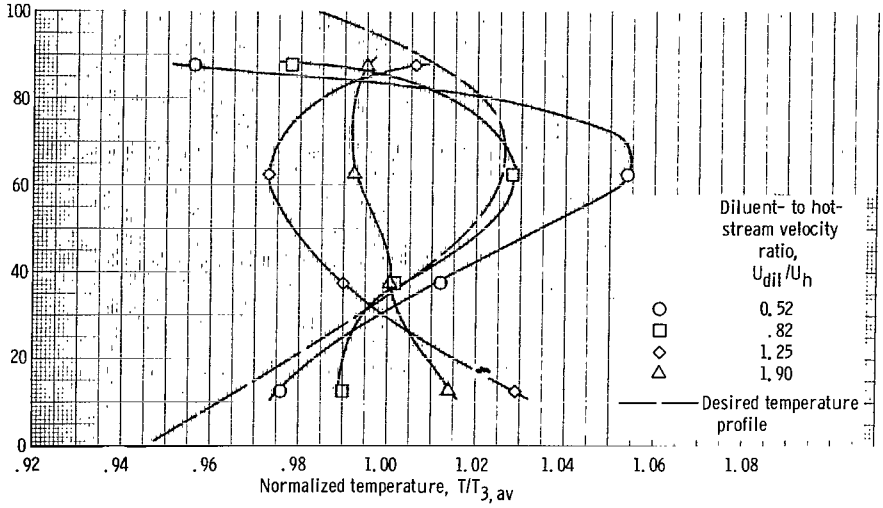

(i) Model E_b (opposing external scoops staggered, turbine blade height spacing).

Figure 11. - Continued.

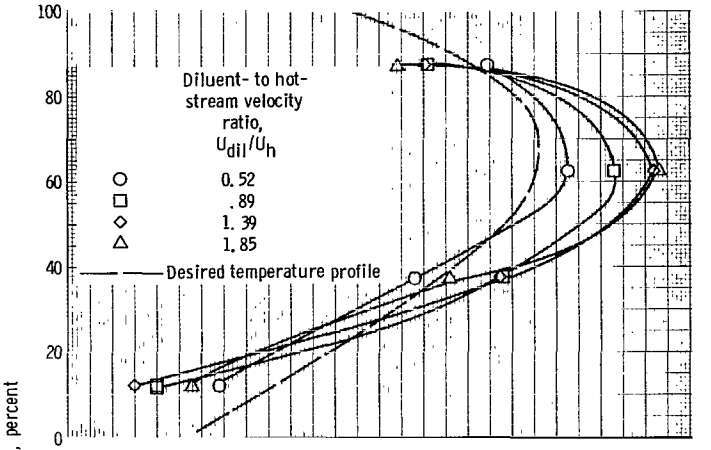

(j) Model B_C (opposing internal chutes in-line, half turbine blade height spacing).

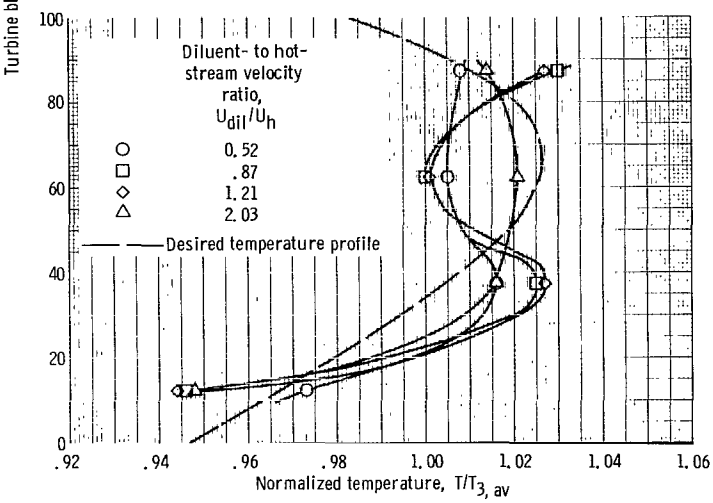

(k) Model C_C (opposing internal chutes staggered, half turbine blade height spacing).

Figure 11. - Continued.

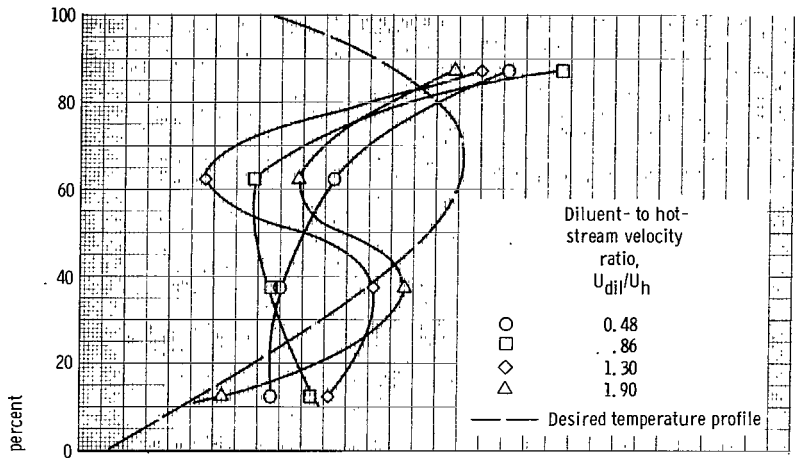

(l) Model D_c (opposing internal chutes in-line, turbine blade height spacing).

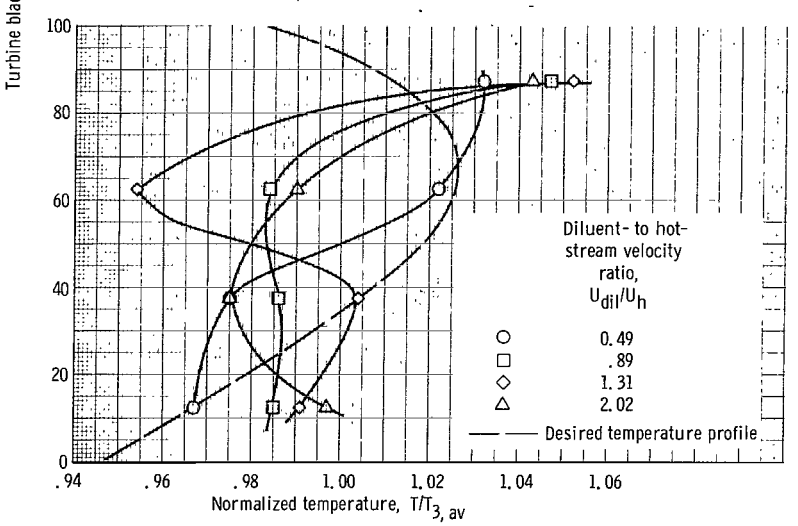

(m) Model E_c (opposing internal chutes staggered, turbine blade height spacing).

Figure 11. - Concluded.

TABLE IV. - EFFECT OF DILUENT- AND HOT-STREAM MASS FLOWS ON MIXING

Nominal diluent- to hot-stream mass flow	Diluent- to hot-stream velocity ratio	Normalized temperature ratio, $T_1/T_{3,av}$	Maximum experimental temperature difference to ideal temperature difference, $\frac{T_1 - T_{3,rad\ max}}{T_1 - T_{3,id}}$
20:80	0.52	1.107	0.488
30:70	.89	1.170	.488
40:60	1.33	1.239	.656
50:50	2.00	1.319	.856

are tabulated in table IV, also. The degree of mixing is reflected in the temperature difference term, which approaches 1 as ideal mixing is attained. As shown by this approach, increased mixing was evident as the velocity ratio was increased. Thus, even through the normalized temperature profiles (fig. 11(a)) for diluent- to hot-stream velocity ratios of 0.52 and 2.00 were similar, comparatively less mixing occurred at the low velocity.

In none of the four cases was the penetration sufficient to eliminate the hot-core experienced with this configuration, however. It was concluded that with the holes closely spaced (half turbine blade height) a coalescing of the jets occurred near the liner wall, resulting in the formation of a layer of cold air which prevented effective penetration and mixing with the hot inner core. Wider spacing of larger holes might have improved the mixing, but no other circular-hole pattern was tested.

Rectangular slots (models B_a to E_a). - The temperature profiles obtained with plain rectangular slots are shown in figure 11(b) for opposing jets in line (model B_a) and in figure 11(c) for opposing jets staggered (model C_a). In models B_a and C_a slot spacing was equal to one-half the turbine blade height, and the total open hole area was nominally equal to that of the circular-hole configuration. For these rectangular hole configurations the intensity of the hot core was somewhat reduced; however, a coalescing of the dilution jets was indicated.

Models D_a and E_a differed from models B_a and C_a in that the slot configuration was changed to six double width slots spaced at a distance equivalent to the turbine blade height. When the slots were changed in this manner a pronounced effect of the diluent- to hot-stream velocity ratio was observed as shown in figures 11(d) and (e), respectively. As the diluent- to hot-stream velocity ratio was increased, an actual reversal from a hot core to a cold core was observed in both models. The high root temperature deviation

from the desired temperature profile as shown in figures 11(d) and (e) is not necessarily poor because it is usually possible to bleed a portion of the cooling air in a film over the turbine blade root or tip to reduce the average local temperature at these positions. From a comparison of figures 11(b) to (e) the radial temperature profile which deviated less from the desired profile was obtained with model E_a at a diluent- to hot-stream velocity ratio of 0.84 (fig. 11(e)).

These results indicate dramatically the effect on outlet-temperature profile of the spacing, velocity, and sizing of the dilution jets.

A comparison of the relative penetration can be made by evaluating and rewriting equation (2) as follows:

$$\frac{Y}{d_j} = 0.87\left(\frac{\rho_{dil}}{\rho_h}\right)^{0.47}\left(\frac{U_{dil}}{U_h}\right)^{0.85}\left(\frac{x}{d_j}\right)^{0.32} \tag{5}$$

The term d_j was evaluated on the basis that the rectangular hole was equivalent to a circle of equivalent hydraulic diameter, and the penetration was based on a distance 2.5 inches (0.064 m) downstream of the hole. The total depth of the test section at this position is 3.32 inches (0.084 m). The calculated depths of penetration of model B_a (narrow slots) and model E_a (wide slots) are presented in table V for a range of diluent- to hot-stream velocity ratios. It is shown that the slots used in this investigation should have allowed the dilution jet to penetrate at least to the center of the test duct. As in the

TABLE V. - CALCULATED PENETRATION DEPTHS FOR NARROW AND WIDE SLOT MODELS

Model	Penetration depth		Diluent- to hot-stream velocity ratio, U_{dil}/U_h
	in.	m	
B_d	0.84	0.021	0.46
	1.37	.035	.82
	1.88	.048	1.21
	2.66	.068	1.85
E_d	1.07	0.021	0.52
	1.58	.040	.82
	2.23	.057	1.25
	3.16	.080	1.90

case with circular holes, rectangular holes closely spaced did not allow sufficient penetration of the dilution jet over the range of diluent- to hot-stream velocity ratios tested. Thus, it has been shown that narrowly spaced holes may leave a hot central core even though the single-hole correlation would predict penetration to the center of the duct. If holes are widely spaced (optimum not established) existing penetration correlations, based on single-hole data, can be used as a guide line in tailoring the temperature profile.

Rectangular slots with external scoops (models B_b to E_b). - The configuration of models B_b to E_b are similar to models B_a to E_a, respectively, except that an external scoop with a turning vane has been added. The outlet-temperature profiles of models B_b to E_b are shown in figures 11(f) to (i). The temperature profiles for model B_b showed no significant improvement over model B_a. The temperature profiles for models C_b, D_b, and E_b were noticeably better than models C_a, D_a, and E_a, respectively, because for similar velocity ratios the experimental temperature profiles more closely matched the ideal profile. The profile which most nearly matched the ideal profile was obtained when the scoops were widely spaced and staggered at a diluent- to hot-stream velocity ratio of 0.82 (model E_b, fig. 11(j)); however, some film cooling would be required to decrease the root temperature.

Internal chute configuration (models B_c to E_c). - The geometric pattern of models B_c to E_c are similar to models B_d to E_d, respectively. The rectangular holes in the upper and lower plates have essentially been elongated, and chutes have been added which terminate in the hot stream. The outlet-temperature profiles of models B_c to E_c are shown in figures 11(j) to (m). For these models quite different trends were observed from those previously discussed. In particular, the best profiles were obtained when internal chutes were closely spaced and in line (model B_c, fig. 11(j)) as compared with external scoops in which the best profiles were obtained with slots widely spaced and staggered (model E_b, fig. 11(i)).

The effect of diluent- to hot-stream velocity ratios on mixing is different for models with internal chutes. The chutes are immersed 1 inch (0.025 m) into the primary zone at a position where the primary duct height is 3.44 inches (0.87 m). At this point the diluent and hot streams are essentially parallel; and mixing is accomplished primarily by velocity differences between the diluent and hot streams (ref. 11) rather than by jet penetration. The velocity of the dilution jet is probably quite different than previous models because the chute probably flows full (i.e., discharge coefficient close to 1); whereas, the rectangular holes are effectively blocked because of lower discharge coefficients. The discharge coefficient effect has not been included, however, since, as previously discussed, the diluent passage velocity approximation rather than the jet discharge velocity has been used for correlation. The high hot-stream velocity and resulting decrease in static pressure result in a high turbulent mixing between the two streams. This

is particularly effective for narrow spacing of the diluent and hot streams. The most uniform profile occurred when opposing chutes were in line with model B_c, at a diluent- to hot-stream velocity ratio of 0.52 (fig. 11(j)).

With six double width scoops, whether in line or staggered, all temperature profiles were relatively poor (figs. 11(l) and (m)). Severe hot spots were experienced at a position corresponding to the tip of the turbine stator. Hot spots with these configurations may be due to hot-gas flow trapped between the wide internal chutes and pushed to the liner wall, the hot gas being unable to mix with the diluent gas which was ducted toward the center of the combustor. It is apparent that the spacing of the diluent and hot streams is critical because mixing was uniform only when the primary and secondary streams were closely spaced with opposing slots in line (model B_c). It should be noted that this conclusion is not in contradiction to the results obtained with previous models because of the quite different method of dilution-air entry.

The internal chute configurations would be difficult to adapt to a specific outlet-temperature profile from mechanical considerations. The experimental results indicate that changes in geometry would be required to change the outlet temperature obtained with narrow-spaced internal chutes because no appreciable change in outlet temperature was obtained with variation in flow splits. When both slot spacing and width were doubled, unacceptable profiles resulted. For a configuration of this type, it is necessary to build a completely new secondary zone in order to evaluate the effect on temperature profile. Therefore, of the configurations tested it was concluded that trial and error matching to a specific outlet-temperature profile would be most time consuming for the internal chute configuration.

An additional consideration with internal chutes is the mechanical hardware immersed in the flame zone. To determine the effect of the hot primary zone on immersed chute metal temperature, the chute was coated with a temperature-sensitive paint for some of the test runs. From paint color changes it was observed that only the lead portion (see fig. 3(b)) of the chute at the plate approached the hot-stream temperature. About 90 percent of the surface remained at a temperature which would be considered acceptable from a structural viewpoint. It might be possible to use film cooling at the leading edge of the chute to maintain an acceptable temperature level.

Effect of Total-Mass Flow and Hot-Stream Temperature

Effect of total mass flow. - The effect of variation in total-mass flow is shown in figure 12 for two configurations (models E_b and B_c) and for a single value of diluent- to hot-stream velocity ratio of approximately 0.90. It would be expected that there might be a small effect on penetration resulting from a Mach number change. At low flows (low

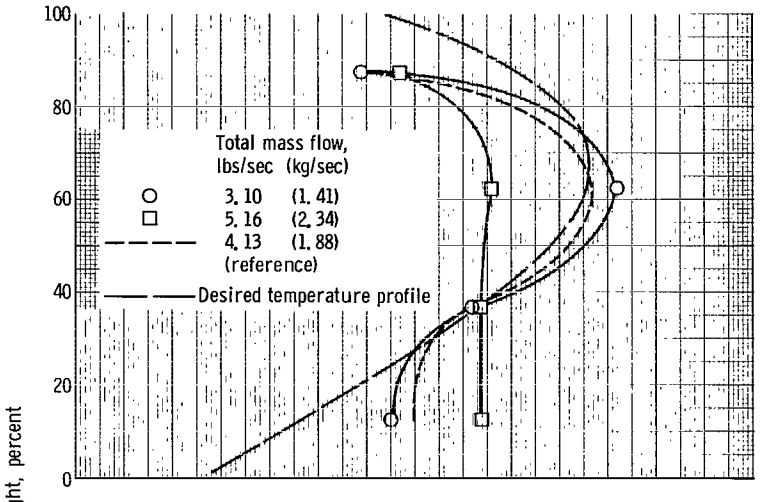

(a) Model E_b (opposing external scoops staggered, turbine blade-height spacing).

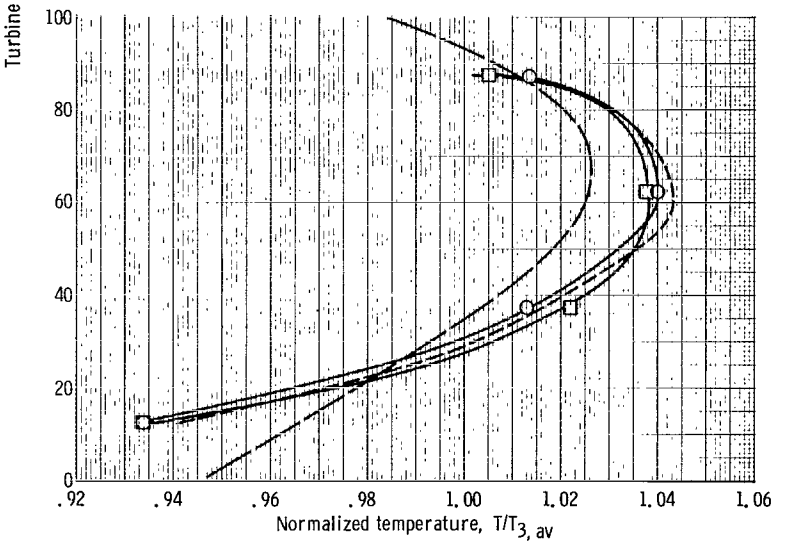

(b) Model B_c (opposing internal chutes in-line, half turbine blade-height spacing).

Figure 12. - Turbine inlet radial temperature profiles at station 3 for three air flow rates. Hot-stream temperature, 1020° R (576 K); diluent-stream temperature, ambient; diluent- to hot-stream velocity ratio, 0.89.

Mach number) there is almost no compressibility effect; whereas, at high flow and higher Mach numbers the compressibility effect becomes more pronounced.

For model E_b (external scoops staggered, turbine blade height spacing) at a mass flow 25 percent more than reference, a relatively flat profile was obtained. At a 25-percent decrease in mass flow, the peak temperature was somewhat higher. Since the test rig had no provision for a controlled exhaust system, the internal pressure rose during increased mass flow rates and dropped during decreased mass flow rates. The effect of variation in diluent- to hot-stream velocity ratio is tabulated in table III. If the variation in velocity ratio is taken into account (i.e., assuming that penetration is a function of the velocity ratio U_{dil}/U_h as shown by eq. (2)), it can be shown from a cross plot of the data at 62.5 percent of the turbine blade height (fig. 11(i)) that the changes in velocity ratio would very nearly account for the change in peak temperature. For model B_c (internal chutes in line, half turbine blade height spacing) in which the dilution stream is introduced almost parallel to the hot-stream flow, there was no marked change in temperature profile.

Effect of hot-stream temperature. - The effect of hot-stream temperature is shown in figure 13 for models E_b and B_c. The combustor hot-stream temperature will vary as the fuel-air ratio; thus, this condition would be experienced in actual engine operation during acceleration and deceleration. As shown in figure 13(a) there was an effect on outlet-temperature profile for the model E_b configuration (external scoops staggered, turbine blade height spacing).

The effect of temperature on penetration can be shown with the aid of equation (5). Substituting in terms of pressure and temperature for density and velocity, penetration varies as

$$\frac{Y}{d_j} = k_3 \left(\frac{T_{dil}}{T_h} \frac{p_h}{p_{dil}} \right)^{0.48} \left(\frac{x}{d_j} \right)^{0.32} \tag{6}$$

The observed change in peak-temperature profile (at 62.5 percent of the turbine blade height) follows the trend as predicted by the jet-penetration expression. A slight effect on the profile might also be due to small changes in the diluent- and hot-stream pressure levels. As the hot-stream temperature was varied, the test section pressure varied because the exhaust area remained constant and there was no control of the exhaust system. For the model B_c configuration (fig. 13(b)) (internal chutes in line, half turbine blade-height spacing) a small effect was also observed.

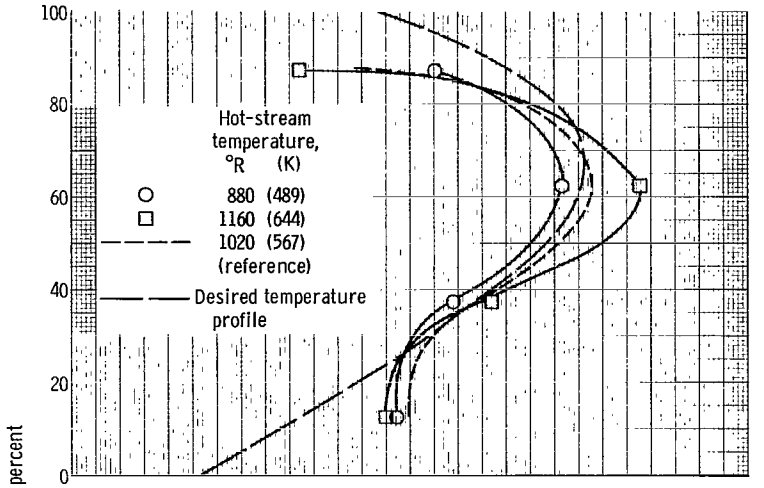

(a) Model E_b (opposing external scoops staggered, turbine blade-height spacing).

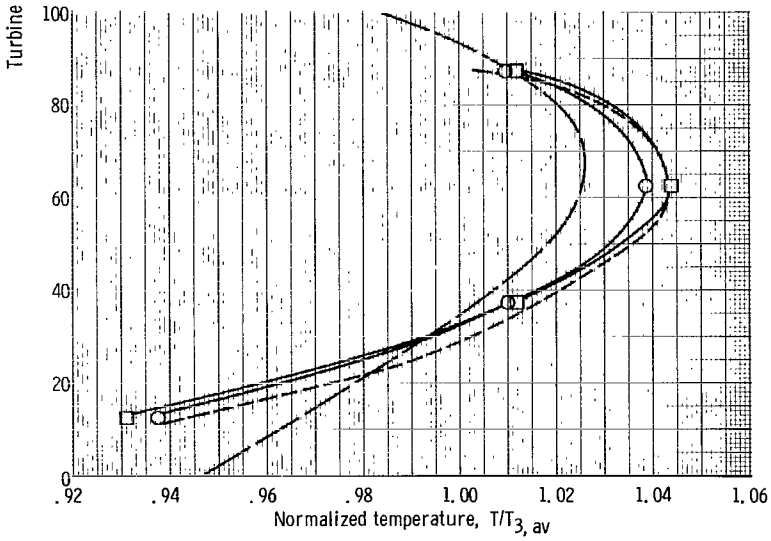

(b) Model B_c (opposing internal chutes in-line, half turbine blade height spacing).

Figure 13. - Turbine-inlet radial-temperature profile at station 3 for three hot-stream temperatures. Total air flow, 4.13 pounds per second (1.88 kg/sec); diluent-air temperature, ambient; diluent- to hot-stream velocity ratio, 0.89.

Lateral-Temperature Profiles

The lateral-temperature profiles characteristic of models E_b and B_c are shown in figure 14 for the reference condition. A reasonable lateral-temperature profile was obtained in both cases without resorting to additional modification. The profile of model E_b is significantly flatter than the profile of model B_c over most of the duct.

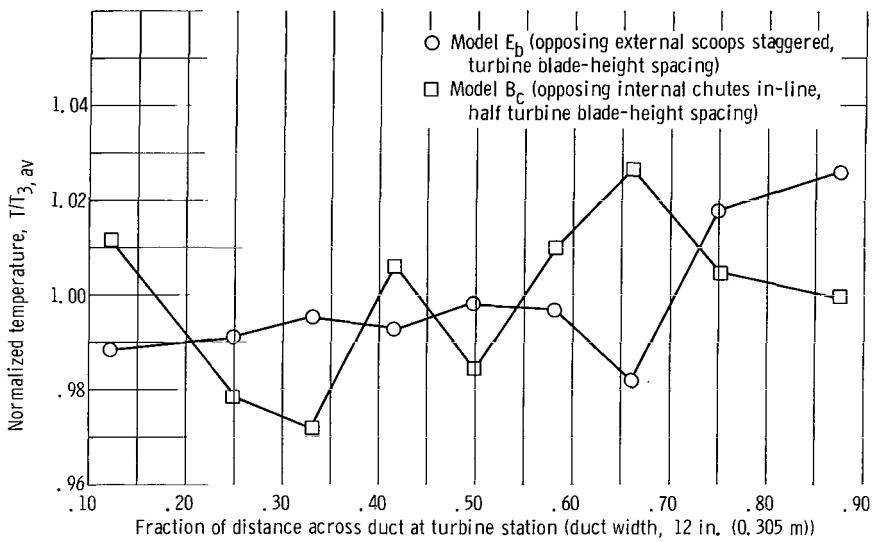

Figure 14. - Turbine-inlet lateral-temperature profile at station 3. Standard flow conditions: total air flow, 4.13 pounds per second (1.88 kg/sec); hot-stream temperature, 1020° R (567 K); diluent-stream temperature, ambient; diluent- to hot-stream velocity ratio, 0.89.

Summary of Outlet-Temperature Profiles

In figure 15 the mixing configurations are compared by compiling all test conditions into a single-band range characteristic of performance as shown by equations (3) and (4) at the maximum temperature observed in the exhaust plane. Two criteria have been selected for comparison of the exhaust temperature: (1) with respect to the turbine stator and (2) with respect to the turbine rotor. The turbine stator is affected by the local maximum permissible temperature that the blade material can tolerate without exceeding design limitations. Because the blade is stationary, hot spots can result in excessive erosion and excessive growth, which results in bending; however, in general, stators are less critical than rotors. The turbine rotor, in turn, is limited by metal fatigue at the blade root, creep along the blade length, and tip erosion. The turbine rotor blade equilibrium temperature will reflect the temperature experienced during rotation, so that the

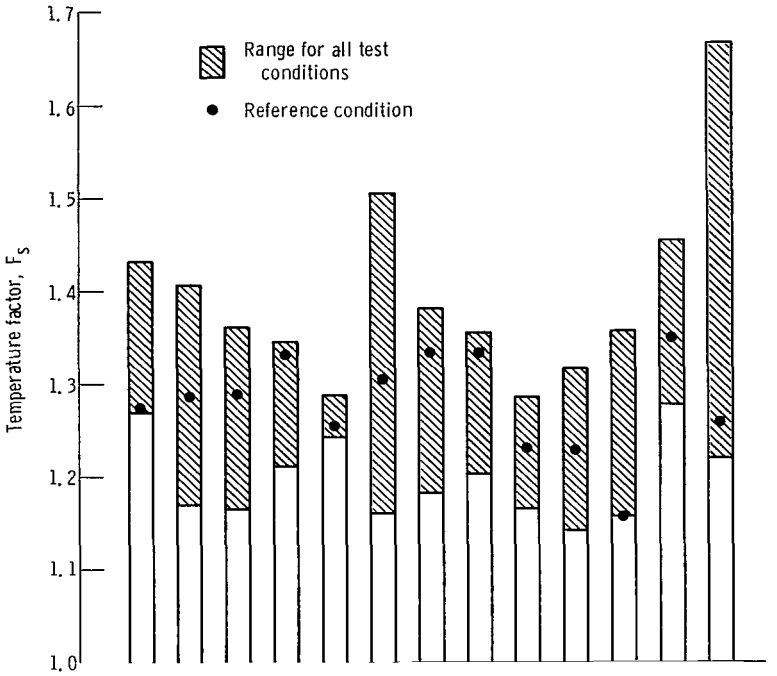

(a) Maximum temperature difference at station 3.

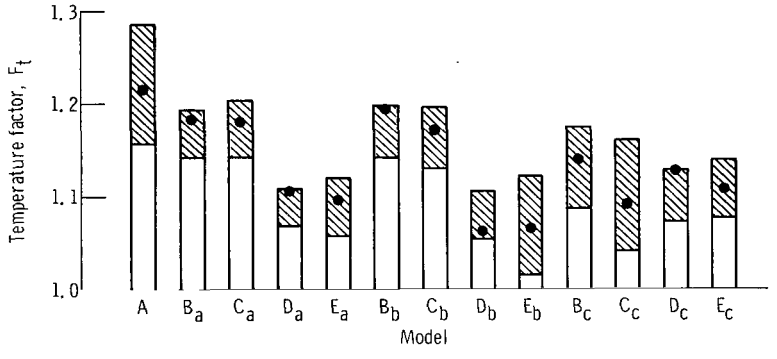

(b) Average temperature difference at station 3.

Figure 15. - Summary of experimental temperature distribution for all test conditions.

average radial temperature profile is most meaningful. A turbine stator comparison is made with respect to the maximum temperature (F_s, eq. (3)) and a turbine rotor comparison is made with respect to the average radial temperature (F_t, eq. (4)) as shown in figure 15.

The range of variation of F_s and F_t (fig. 15) represent the effect of variations in flow split between the diluent and hot stream, inlet temperature, and total-mass flow. As shown, some configurations are particularly well adapted to handling a wide range of conditions without adversely affecting the turbine. In addition to a narrow range, it is

also desirable to have a low numerical value of F_s and F_t. The value of F_s for the stator position is higher than F_t at the turbine position because of the averaging of peak temperature by the rotating wheel.

Total-Pressure Losses

Diluent holes. - Pressure loss as related to combustor performance is usually defined as the ratio of the difference between the total pressure at the compressor outlet and the turbine inlet to total pressure at the compressor outlet. It is not possible to relate the pressure loss in this manner in this investigation because of the geometry of the test section and the separation of the hot and diluent streams. Of the two streams the diluent-air stream is of greater interest because it reflects the pressure drop incurred across the diluent holes. As an indication of performance, the ratio of the difference between the total pressure in the diluent stream and the turbine inlet to the total pressure in the diluent stream was used. This total pressure drop is shown in figure 16 as a function of diluent- to hot-stream velocity ratio for all configurations. Also included in figure 16 is a calculated pressure drop for comparison with experimental data.

It is necessary to make a number of assumptions in order to calculate a pressure drop of the diluent stream. It was assumed that the velocity head of the diluent stream was lost and that there were no mixing losses. These assumptions are not quite true, but they should generally suffice for an approximation. In the test configuration the diluent holes correspond to a position where there is no flow past the hole (zero cross flow) so that the actual discharge coefficient associated with the hole would be constant. When it is assumed that the hot-stream velocity has no effect on the discharge coefficient, use was made of the extensive compilation of discharge coefficient data in the literature. As previously mentioned, a discharge coefficient of 0.55 was used for circular holes. Rectangular holes with the longest axis parallel to the flow have been shown to have a discharge coefficient of 0.58 (ref. 7). This discharge coefficient was used with plain rectangular holes and with external scoops attached because the addition of an external scoop at zero cross flow is primarily influential in directing the diluent jet rather than changing the discharge coefficient. A discharge coefficient of 1 was selected for the case of internal chutes because no information on a hole configuration of this type is presented in the literature. It should be noted, however, that, because of the large open area in the plate wall and because of the enclosed chute, it is quite reasonable to expect that the flow would only be limited by the cross-sectional area of the discharge. Using the actual diluent-stream total pressure (in practice it was higher than the atmospheric pressure assumed for initial design calculations) the calculated pressure loss was obtained.

The calculated pressure loss is, in general, comparable to the experimental pressure

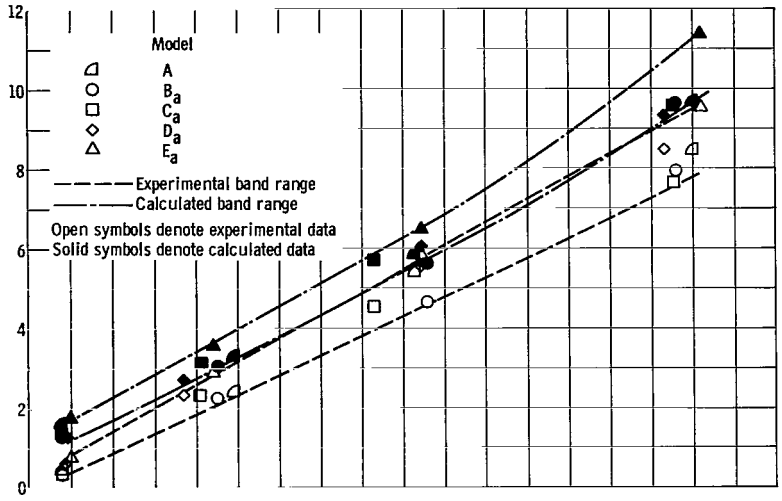

(a) Plain circular and rectangular holes.

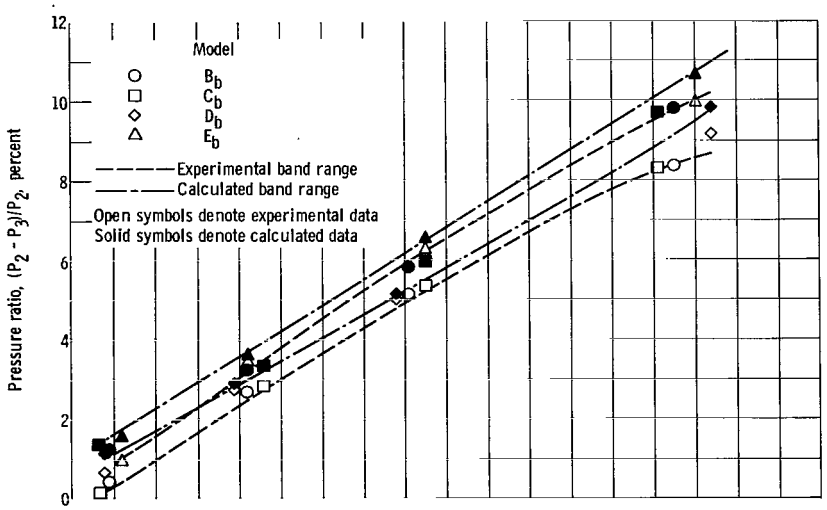

(b) Rectangular holes with external scoops.

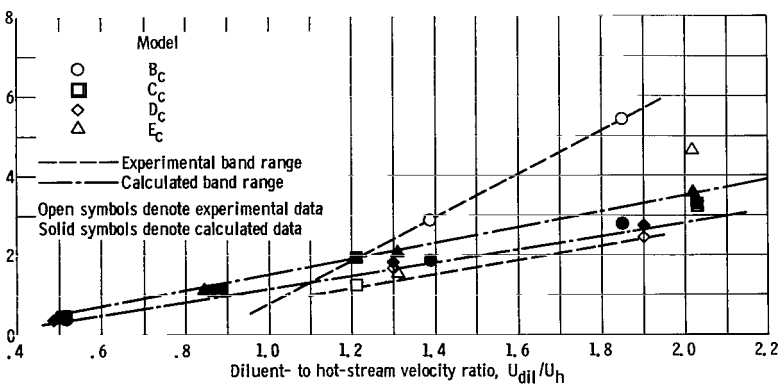

(c) Rectangular holes with internal chutes.

Figure 16. - Total pressure loss of diluent to mixed streams for test configurations. Fixed total-mass flow, 4.13 pounds per second (1.88 kg/sec); hot-stream temperature, 1020° R (567 K); diluent-stream temperature, ambient.

loss for circular holes, rectangular holes, and rectangular holes with external scoops (figs. 16(a) and (b)). The models with external scoops appear to have a somewhat higher pressure loss than their counterparts without external scoops.

The configurations with internal chutes (fig. 16(c)) appear to be inconsistent with expected operation in that the diluent passage total pressure observed experimentally was lower than the outlet total pressure for values of U_{dil}/U_h less than 1. The hot duct is partially blocked because of the internal chutes. This, in turn, results in a high velocity pass the chute and diluent-air discharge port. Consequently, at low diluent flow rates ($U_{dil}/U_h < 1$) it appears that the combination of increased primary flow (total-mass flow constant) and additional velocity increase has produced an aspirating effect in the diluent-air passage. This condition could be detrimental in an actual configuration because of the possible reversal of the hot gases into the dilution stream via primary air holes. At higher diluent flows (decreased hot-stream velocity) the noteable reduction of the experimental pressure loss with internal chutes appears to agree fairly well with the calculated pressure loss.

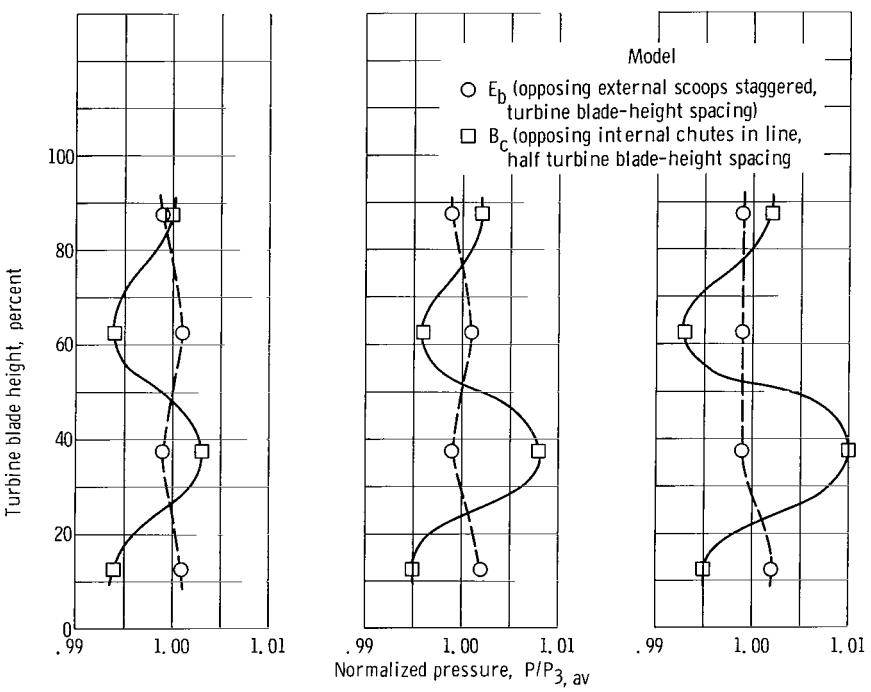

Figure 17. - Station 3 inlet radial-pressure profiles for three total air-flow rates. Hot-stream temperature, 1020° R (567 K); diluent-stream temperature, ambient; diluent- to hot-stream velocity ratio, 0.89.

Outlet-total-pressure profiles. - The average outlet-total-pressure profiles of two mixing configurations are compared in figure 17 for three total air-flow conditions. The pressure readings have been normalized to the average total pressure at the mixing zone exhaust station. As shown in figure 17 model E_b had a relatively uniform exhaust total-pressure profile. The average outlet-total-pressure profile from model B_c (which was typical of the internal chute configuration, in general) had a rather pronounced variation which was intensified by increased mass flow. Since no appreciable pressure profile gradients were noted when the flame tube area was not blocked, it was deduced that the blockage was responsible for this effect.

SUMMARY OF RESULTS

The following information was obtained as part of an experimental evaluation of 13 dilution-jet entry schemes suitable for advanced turbine engines utilizing short-length combustors.

1. The configurations which provided the most uniform outlet temperature profiles included all three of the basic types of dilution-air entry apertures, flush holes, holes with external scoops, and holes with internal chutes. Hence, no clear superiority is indicated for any type of dilution aperture, and a good temperature profile can be obtained with any of the three basic apertures.

2. Mixing was improved for flush holes of rectangular shape both with or without external scoops by enlarging the holes and increasing the hole spacing. A spacing equivalent to the turbine blade height produced a variation ranging from a hot to a cold central core as the ratio of diluent- to hot-stream velocity was increased. A spacing of one-half the turbine blade height produced a hot central core for all ratios of diluent- to hot-stream velocity ratio.

3. For rectangular holes with internal chutes the use of narrow, closely spaced holes was beneficial. In this case more widely spaced larger holes produced temperature profiles that were hot at both tip and root. The difference in profiles obtained using opposed and interleaved jets was more marked for internal chutes than for other geometries. The effect of diluent- to hot-stream velocity ratio was less marked.

4. Experimental total-pressure losses of the diluent stream injected through plain holes and external scoops attached to plain rectangular holes agree fairly well with calculated losses. With internal chutes attached to plain rectangular holes, it is possible to achieve a marked decrease in dilution-air total-pressure loss without accompanying deterioration in the outlet-temperature profile. The lower dilution-air pressure loss

does not necessarily result in a lower overall combustor pressure loss. Because the pressure loss in the primary stream was not measured, it cannot be concluded that internal chutes will provide lower overall pressure loss.

Lewis Research Center,
National Aeronautics and Space Administration,
Cleveland, Ohio, March 21, 1968,
720-03-01-80-22.

APPENDIX - SYMBOLS

a_1, b_1, c_1 a_2, b_2, c_2	exponents
d	diameter
F_s	temperature factor, $(T_{3,max} - T_2)/(T_{3,av} - T_2)$, see eq. (3)
F_t	temperature factor, $(T_{3,rad\ max} - T_2)/(T_{3,av} - T_2)$, see eq. (4)
k_1, k_2, k_3	constants
M	Mach number
$\dot{m}$	mass flow
N	number of holes
P	total pressure
p	static pressure
S	size of hole
T	total temperature
U	velocity
x	distance from a reference point
Y	effective penetration
z	hole spacing, center to center
ρ	density

Subscripts:

a	plain rectangular holes
av	average
b	external scoops
c	internal chutes
dil	diluent gas
h	hot gas
id	ideal
j	jet
max	maximum
rad	average radial profile
s	stator
T	total
t	turbine
1	instrumentation plane 1, hotstream
2	instrumentation plane 2, diluent stream
3	instrumentation plane 3, turbine stator

REFERENCES

1. Anon.: The Design and Performance Analysis of Gas-Turbine Combustion Chambers. Vol. 1. Theory and Practice of Design. Rep. No. 1082-1, Northern Research and Engineering Corp., Cambridge, Mass., 1964.

2. Lefebvre, A. H.; and Norster, E. R.: A Design Method for the Dilution Zones of Gas Turbine Combustion Chambers. Rep. No. CoA-AERO-169, College of Aeronautics, Cranfield, England, Feb. 1966.

3. Lefebvre, A. H.: Progress and Problems in Gas-Turbine Combustion. Tenth Symposium (International) on Combustion. The Combustion Institute, 1965, pp. 1129-1137.

4. Stewart, D. G.: Scaling of Gas Turbine Combustion Systems. Selected Combustion Problems, II: Transport Phenomena, Ignition, Altitude Behaviour and Scaling of Aeroengines. Butterworths Scientific Publ., 1956, pp. 384-413.

5. Hawthorne, W. R.; Rodgers, G. F. C.; and Zaczek, B. Y.: Mixing of Gas-Streams - The Penetration of a Jet of Cold Air Into a Hot Stream. Tech. Note Eng. 271, Royal Aircraft Establishment, Mar. 1944.

6. Dittrich, Ralph T.; and Graves, Charles C.: Discharge Coefficients for Combustor-Liner Air-Entry Holes. I - Circular Holes with Parallel Flow. NACA TN 3663, 1956.

7. Dittrich, Ralph T.: Discharge Coefficients for Combustor-Liner Air-Entry Holes. II - Flush Rectangular Holes, Step Louvers, and Scoops. NACA TN 3924, 1958.

8. Clarke, J. S.; and Jackson, S. R.: General Considerations in the Design of Combustion Chambers for Aircraft and Industrial Gas Turbines. Paper presented at International Congress and Exposition of Automotive Engineering, SAE, Detroit, Mich., Jan. 8-12, 1962.

9. Norgren, Carl T.: Design and Performance of an Experimental Annular Turbojet Combustor with High-Velocity-Air Admission Through One Wall. NASA Memo 12-28-58E, 1958.

10. Anon.: The Design and Performance Analysis of Gas-Turbine Combustion Chambers. Vol. II. Design Methods and Development Techniques. Rep. No. 1082-2, Northern Research and Engineering Corp., Cambridge, Mass., 1964.

11. Korst, H. H.; and Chow, W. L.: Non-Isoenergetic Turbulent ($Pr_t = 1$) Jet Mixing Between Two Compressible Streams at Constant Pressure. Illinois Univ. (NASA CR-419), Apr. 1966.

NATIONAL AERONAUTICS AND SPACE ADMINISTRATION
WASHINGTON, D.C. 20546

OFFICIAL BUSINESS

FIRST CLASS MAIL

POSTAGE AND FEES PAID
NATIONAL AERONAUTICS AND
SPACE ADMINISTRATION

"The aeronautical and space activities of the United States shall be conducted so as to contribute . . . to the expansion of human knowledge of phenomena in the atmosphere and space. The Administration shall provide for the widest practicable and appropriate dissemination of information concerning its activities and the results thereof."

—NATIONAL AERONAUTICS AND SPACE ACT OF 1958

NASA SCIENTIFIC AND TECHNICAL PUBLICATIONS

TECHNICAL REPORTS: Scientific and technical information considered important, complete, and a lasting contribution to existing knowledge.

TECHNICAL NOTES: Information less broad in scope but nevertheless of importance as a contribution to existing knowledge.

TECHNICAL MEMORANDUMS: Information receiving limited distribution because of preliminary data, security classification, or other reasons.

CONTRACTOR REPORTS: Scientific and technical information generated under a NASA contract or grant and considered an important contribution to existing knowledge.

TECHNICAL TRANSLATIONS: Information published in a foreign language considered to merit NASA distribution in English.

SPECIAL PUBLICATIONS: Information derived from or of value to NASA activities. Publications include conference proceedings, monographs, data compilations, handbooks, sourcebooks, and special bibliographies.

TECHNOLOGY UTILIZATION PUBLICATIONS: Information on technology used by NASA that may be of particular interest in commercial and other non-aerospace applications. Publications include Tech Briefs, Technology Utilization Reports and Notes, and Technology Surveys.

Details on the availability of these publications may be obtained from:

SCIENTIFIC AND TECHNICAL INFORMATION DIVISION

NATIONAL AERONAUTICS AND SPACE ADMINISTRATION

Washington, D.C. 20546